HDL-TR-1598

FLUERICS 32. AN ANALYTICAL MODEL FOR THE RESPONSE OF FLUERIC WALL ATTACHMENT AMPLIFIERS

by

John M. Goto

Tadeusz M. Drzewiecki

June 1972

U.S. ARMY MATERIEL COMMAND
HARRY DIAMOND LABORATORIES
WASHINGTON, D.C. 20438

67

The findings in this report are not to be construed as an official Department of the Army position unless so designated by other authorized documents.

Citation of manufacturers' or trade names does not constitute an official indorsement or approval of the use thereof.

Destroy this report when it is no longer needed. Do not return it to the originator.

DOCUMENT CONTROL DATA - R & D

(Security classification of title, body of abstract and indexing annotation must be entered when the overall report is classified)

1. ORIGINATING ACTIVITY (Corporate author) Harry Diamond Laboratories Washington, D.C. 20438	2a. REPORT SECURITY CLASSIFICATION Unclassified 2b. GROUP
3. REPORT TITLE FLUERICS 32. AN ANALYTICAL MODEL FOR THE RESPONSE OF FLUERIC WALL-ATTACHMENT AMPLIFIERS	
4. DESCRIPTIVE NOTES (Type of report and inclusive dates)	
5. AUTHOR(S) (First name, middle initial, last name) John M. Goto and Tadeusz M. Drzewiecki	
6. REPORT DATE June 1972	7a. TOTAL NO. OF PAGES 76 7b. NO. OF REFS 16
8a. CONTRACT OR GRANT NO. b. DA-1T061102833B c. AMCMS Code: 501B.11.71200 d. HDL Proj: 3FL31	9a. ORIGINATOR'S REPORT NUMBER(S) HDL-TR-1598 9b. OTHER REPORT NO(S) (Any other numbers that may be assigned this report)
10. DISTRIBUTION STATEMENT Approved for public release; distribution unlimited	
11. SUPPLEMENTARY NOTES	12. SPONSORING MILITARY ACTIVITY U.S. Army Materiel Command

13. ABSTRACT

A two-dimensional, incompressible model is examined for the response of laminar and turbulent attached jets to arbitrary control pressures applied to either or both control ports of a flueric bistable amplifier. Effects of the nonlinear, lumped-parameter, inductive and resistive supply, control, vent, and output lines, and effects of the wall opposite the attachment wall are considered. All geometric parameters such as wall angle and offset, vent location, line size, and nozzle width may be varied.

Switching time data for seven different geometries and steady-state attachment-point data for both closed and open control ports, as well as the response of an actual amplifier compare favorable with analytical predictions. The response of a laminar jet to a ramp input pressure change is also given. The analytical results are in good agreement with experimental data. These results indicate that the analytical model is valid and that it can be used as a basis in designing future flueric amplifiers.

DD FORM 1 NOV 65 1473 REPLACES DD FORM 1473, 1 JAN 64, WHICH IS OBSOLETE FOR ARMY USE.

14. KEY WORDS	LINK A		LINK B		LINK C	
	ROLE	WT	ROLE	WT	ROLE	WT
Amplifier	8	3				
Digital devices	8	3				
Flow	8	3				
Fluidics	8	3				
Fluerics	8	3				
Fluid mechanics	8	3				
Jets	8	3				
Lines	8	3				
Logic elements	8	3				

AD

DA-1T061102833B
AMCMS Code: 501B.11.71200
HDL Proj: 3FL31

HDL-TR-1598

FLUERICS 32. AN ANALYTICAL MODEL FOR THE RESPONSE OF FLUERIC WALL ATTACHMENT AMPLIFIERS

by

John M. Goto

Tadeusz M. Drzewiecki

June 1972

U.S. ARMY MATERIEL COMMAND

HARRY DIAMOND LABORATORIES

WASHINGTON, D.C. 20438

ABSTRACT

A two-dimensional, incompressible model is presented for the response of laminar and turbulent attached jets to arbitrary control pressures applied to either or both control ports of a flueric bistable amplifier. Effects of the nonlinear, lumped-parameter, inductive and resistive supply, control, vent, and output lines, and effects of the wall opposite the attachment wall are considered. All geometric parameters such as wall angle and offset, vent location, line size, and nozzle width may be varied.

Switching time data for seven different geometries and steady-state attachment-point data for both closed and open control ports, as well as the response of an actual amplifier compare favorably with analytical predictions. The response of a laminar jet to a ramp input pressure change is also given. The analytical results are in good agreement with experimental data. These results indicate that the analytical model is valid and that it can be used as a basis in designing future flueric amplifiers.

Preceding page blank

ACKNOWLEDGMENT

The authors gratefully acknowledge the help of Charles N. Milewski and John M. Delawter who fabricated the HDL test models.

CONTENTS

TABLES

FIGURES

1. INTRODUCTION

A fundamental component of many fluidic systems is the wall-attachment amplifier. In spite of its importance and the great deal of work expended on it, the design of this amplifier has been based primarily on cut-and-try techniques because a sufficiently accurate analytical model has not been available. The advance toward a design theory of a wall-attachment amplifier began with Bourque and Newman[1] who used the attachment bubble control volume concept to determine the point of reattachment. This concept, with many variations, has proved fruitful, and by its use, the theoretical design has been extended by Wada and Shimizu[2] and Kimura and Mitsuoka.[3] Time-dependent analyses have been presented recently by Epstein,[4] Wilson,[5] Lush,[6-8] and Goto and Drzewiecki.[9] The references cited by Epstein adequately summarize the previous work.

In this paper, we present a practical analytical model for the internal dynamics and switching characteristics of a flueric wall-attachment amplifier with a sharp splitter. This model improves on our previous one,[9] because the effects of the splitter and outputs are considered as well as the fact that the jet is allowed to attach to the opposite wall. In addition to discussing the improved model, we also give an account of our previous models. We believe that this is worthwhile for two reasons: (1) the steps through which the present model has evolved are clarified, and (2) the theory and data on the simple model should prove useful in formulating theories for other fluidic designs.

The analysis for the inner portion of the amplifier is based on a fully developed two-dimensional, incompressible laminar or turbulent jet. It is reasonable to postulate fully developed jet flow in the

---

[1] Bourque, C. and Newman, B.G., "Reattachment of a Two-Dimensional, Incompressible Jet to an Adjacent Flat Plate," The Aeronautical Quarterly, Vol. XI, August 1960.

[2] Wada, T. and Shimizu, A., "Experimental Study of Attaching Jet Flow on an Inclined Flat Plate with Small Offset," Proc. 2nd IFAC Symposium on Fluidics, Prague, 1971.

[3] Kimura, M. and Mitsuoka, T., "Analysis and Design of Wall Attachment Devices by a Jet Model of Unsymmetrical Velocity Profile," Proc. IFAC Symposium on Fluidics, London, 1968.

[4] Epstein, M., "Theoretical Investigation of the Switching Mechanism in a Bistable Wall Attachment Fluid Amplifier," ASME Publication 70-Flcs-3, June 1970, also J. Basic Eng., pp. 55-62, March 1971.

[5] Wilson, M.P., Jr., "The Switching Process in Bistable Fluid Amplifiers," ASME Publication 69-Flcs-28, June 1969.

[6] Lush, P.A., "Investigation of the Switching Mechanism in a Large Scale Model of a Turbulent Reattachment Amplifier," Second Cranfield Fluidics Conference, Cam-Bridge, England, 1967.

[7] Lush, P.A., "A Theoretical and Experimental Investigation of the Switching Mechanism in a Wall Attachment Fluid Amplifier," Proc. IFAC Symposium on Fluidics, London, 1968.

[8] Lush, P.A., "The Development of a Theoretical Model for the Switching Mechanism of a Wall Attachment Fluid Amplifier," Ph.D. Thesis, University of Bristol, Dept. of Aero. Engr., September 1968.

[9] Goto, J.M. and Drzewiecki, T.M., "Reattached Jet Response to Input Pressure in a Non-Loaded Fluidic Bistable Configuration," Fifth Cranfield Fluidics Conference, Uppsala, Sweden, June 1972.

interaction chamber as long as control port gaps are present. Note, however, that prior analyses assuming a fully developed laminar jet profile with no control port gap have grossly overestimated the attachment point distance for geometries having small wall angles and zero offset (Comparin, et al.[10]). When there is no control port gap, one might think that the flow never fully separates and therefore attaches very quickly. Qualitative water table observations show that when a control gap is provided, the attachment point moves far downstream, more in agreement with the fully developed jet predictions. Thus, the use of a fully developed jet analysis is justified only when control port gaps exist. Similar arguments apply to the turbulent jet. It is interesting to note that the geometric scaling laws for turbulent confined flows are unknown, so that for turbulent jets, the analysis should hold only when fully developed turbulence is established. As long as that criterion is met, or when the jet is laminar, there should not be any physical-size limitations on the devices for which the theory holds.

The outer portion of the amplifier model consists of channels for the supply, control, vent, and output lines. The lines are characterized as lumped-parameter inductive and nonlinear resistive components. The lines are coupled to the inner region pressures; therefore, flows through all lines vary with changes of jet position. Most of the basic assumptions have been used extensively by previous authors.[1-9] Additional assumptions about the nature of the flow were necessary for this model because variable line flows and the vortex in the attachment bubble were considered. Furthermore, low-offset cases may be studied by allowing the jet to flow along the opposite wall as opposed to terminating the process as soon as the jet touches the opposite wall.[4,6] A sharp splitter allows the assumption of a lossless peeling off of momentum flux from the jet, and the motion of the jet past the controls permits the calculation of control resistance based on the jet-wall spacing, if necessary.

2. FORMULATION

The analysis is formulated for the model shown in figures 1 and 2. Distances x and y are referred to the geometric axis of symmetry and the supply nozzle exit plane, whereas n and s are referred to the curving jet centerline. A distance n is measured normal to the jet centerline at some jet centerline arc length s. The Goertler velocity profile (Schlichting,[11] p. 606) is assumed for the turbulent supply jet and the Schlichting profile (Schlichting,[11] p. 167) for the laminar jet. The turbulent profile is independent of Reynolds number (Re) but contains a jet-spread parameter, whereas the laminar profile is Reynolds-number-dependent, containing no undetermined parameters.

The centerline of the jet is chosen as the streamline most significant to the downstream temporal position of the jet. In general, the subscripts a and i denote the active (attached) and inactive (opposite) side of the flueric amplifier, respectively. The extended jet centerline intersects the attachment wall at the point denoted by the subscript w. All unprimed quantities are dimensionless. Quantities with dimensions of length are normalized with respect to the supply nozzle width b_+'. (The subscript + refers to an invariant supply, source, or

[10] Comparin, R.A., Jenkins, W.C. and Moore, R.B., "Jet Reattachment at Low Reynolds Number and Moderate Aspect Ratios," ASME Publication 67-FE-25, May 1967.

[11] Schlichting, H., Boundary Layer Theory, McGraw-Hill, New York, 1960.

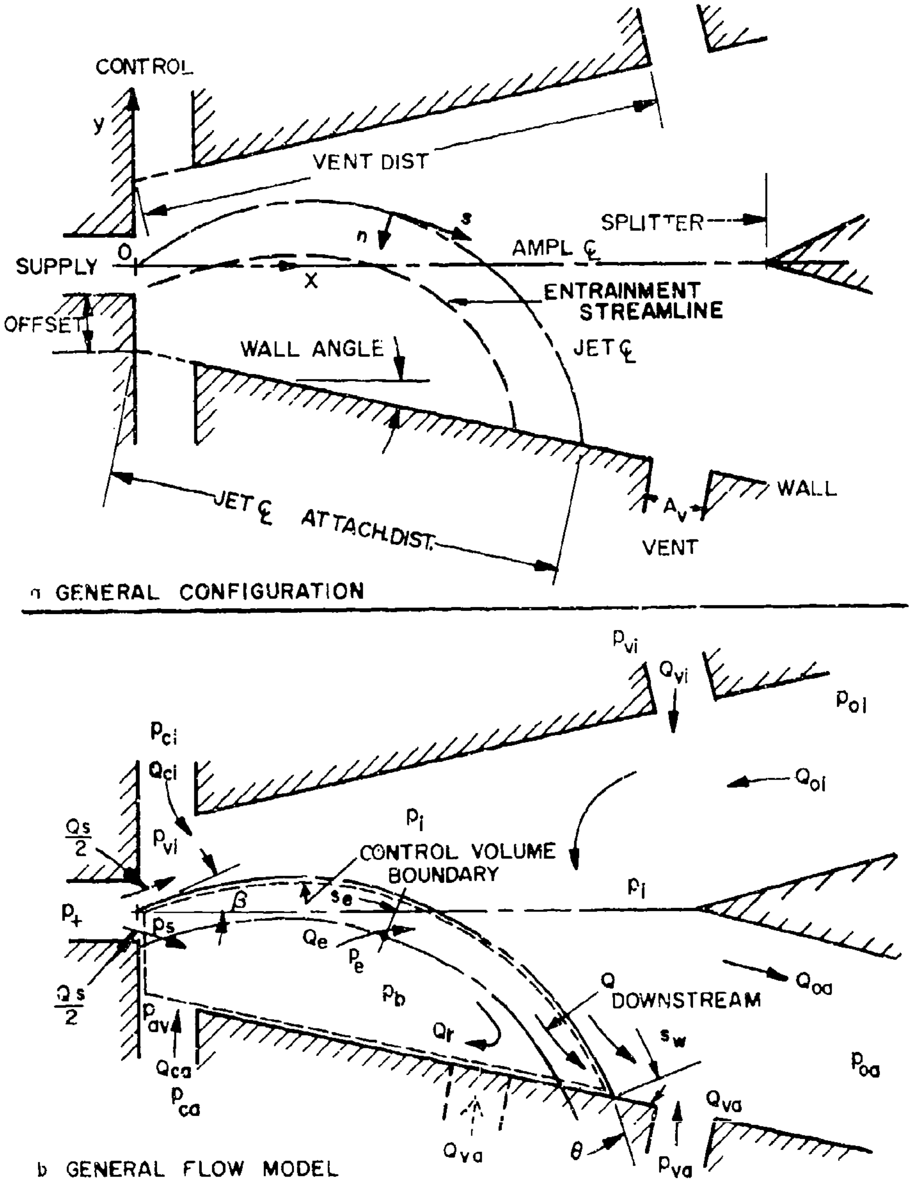

Figure 1. Attachment model

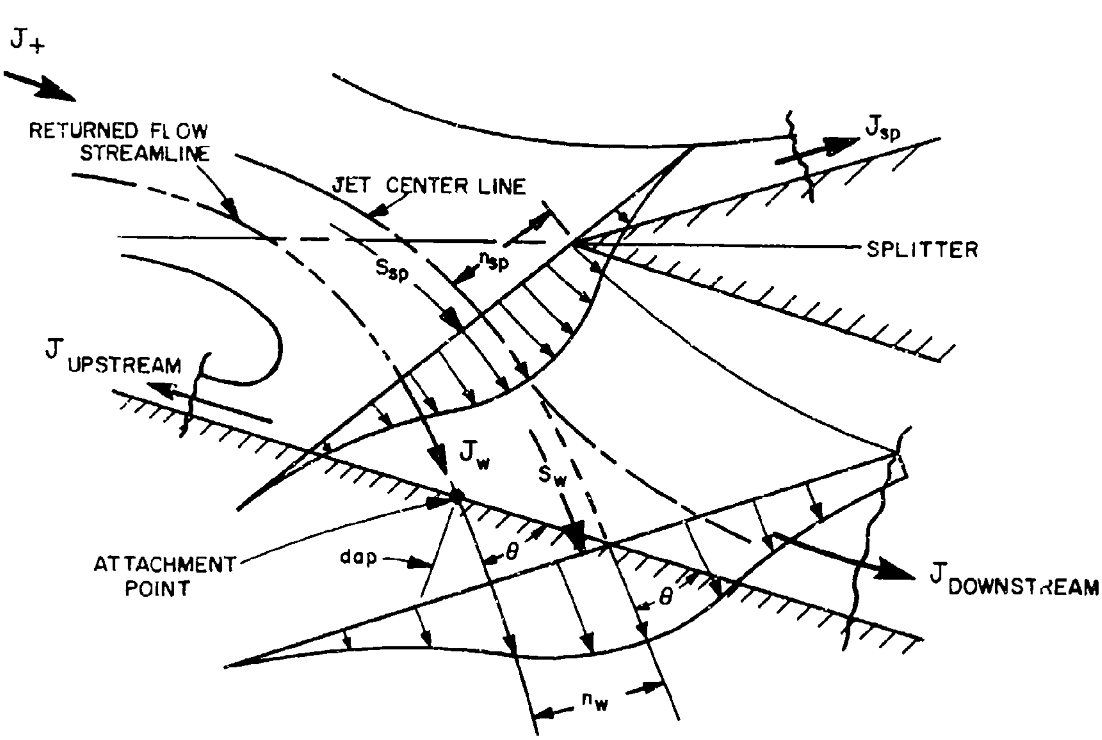

Figure 2. Momentum at attachment point

reference condition.) Areas and volumes are per unit depth and are normalized by b_+' and $b_+'^2$ respectively. All pressures are gage. Static pressures are normalized with respect to the supply total pressure p_+'. Since the supply nozzle exit pressure p_s' is not a constant in this model, the supply flow per unit depth Q_s' is not constant, and so for volumetric flow normalization purposes, an arbitrary constant flow Q_+' is defined by the following relationship to the actual supply total pressure p_+':

$$Q_+' = b_+'\sqrt{2p_+'/\rho'} \tag{1}$$

where ρ' is the fluid density. Velocities u' are normalized with respect to $u_+' = Q_+'/b_+'$. Note that flow is per unit depth. The Reynolds number Re_+ is defined as

$$Re_+ = \frac{b_+'}{\nu'}\sqrt{\frac{2p_+'}{\rho'}}$$

where ν is the kinematic viscosity. Subsequent equations involving flow and velocity will differ from those of previous analyses by some factor of the supply flow Q_s'. Time t' is normalized with $b_+'^2/Q_+' = t_+'$ Ordinarily, t_+' is the transport time based on the supply nozzle width (i.e., the time required for a fluid particle moving at the supply jet exit velocity u_s' to travel a distance of one nozzle width). However, $b_+'/u_s' = b_+'^2/Q_s'$ is the actual transport time, but it has lost its significance because it varies in a time-dependent process.

Figure 1b shows all the flows and their respective pressure differences. The bubble and opposite-side pressures are represented by mean pressures p_b and p_i, and compensation for the bubble pressure distribution is made by assuming that the active control exit pressure is equal to $P_{av} = (p_b + p_i)/2$. The supply jet exits to an interaction region that has a pressure lower than ambient, and it is assumed that the exit pressure of the supply can be represented by an average pressure $p_s = (p_{av} + p_i)/2$ (see fig. 1b). Thus, the supply and control flows are coupled to the interaction region by these pressures.

2.1 Supply Jet Velocity Profile Equations, u

In terms of the coordinates s and n, the normalized form for the fully developed two-dimensional incompressible jet velocity profile is

$$u = k_1 \operatorname{sech}^2 k_2 n \tag{2}$$

where

$$\left.\begin{aligned} k_1 &= Q_s\left(\frac{3\sigma}{4(s + s_{vo})}\right)^{1/2} \\ k_2 &= \frac{\sigma}{s + s_{vo}} \end{aligned}\right\} \text{TURBULENT} \tag{3a}$$

$$\left.\begin{aligned} k_1 &= C_1 Q_s\left(\frac{Re_+ Q_s}{s + s_{vo}}\right)^{1/3} \\ k_2 &= C_2\left(\frac{Re_+ Q_s}{s + s_{vo}}\right)^{2/3} \end{aligned}\right\} \text{LAMINAR} \tag{3b}$$

$$C_1 = 0.4543 \qquad C_2 = 0.2752$$

and s is the distance measured along the curving jet centerline. The unknowns in eq (2) and (3) are the supply flow Q_s, the point source distance s_{vo}, and the fluid velocity u.

The turbulent jet spread parameter σ must be specified. When applied to attached jets, it is usually assigned a value most consistent with experimental data. The work of Lush[6-8] and Kimura and Mitsuoka indicates that $7.67 < \sigma < 14$. A constant value of 10 has been chosen for use in this model.

2.2 Attachment Bubble Volume, V_b

The jet centerline arc, the offset, and the attachment walls define the control volume of the attachment bubble (fig. 1b). The flows crossing the control volume boundaries are one-half of the total supply flow $Q_s/2$, the control flow Q_{ca}, the vent flow Q_{va}, and the downstream flow $Q_{downstream}$. There is no vent flow Q_{va} into the bubble if the jet is attached upstream of the vent. The downstream flow is determined by going inside the control volume and calculating the difference between returned flow Q_r and the sum of the half-supply flow $Q_s/2$ and entrained flow Q_e. The differential equation governing the time rate of change of the bubble volume V_b is the continuity equation

$$\frac{dV_b}{dt} = \frac{Q_s}{2} + Q_{ca} + Q_{va} - Q_{downstream}$$

but

$$Q_{downstream} = \frac{Q_s}{2} + Q_e - Q_r$$

so that

$$\frac{dV_b}{dt} = Q_{ca} - Q_e + Q_r + Q_{va} \qquad (4)$$

This is then a capacitive effect caused by bubble volume change.

The difference between the returned and entrained flows is obtained by integrating the assumed jet velocity profile from the entrainment streamline to the attachment streamline at the attachment point. This results in

$$Q_e - Q_r = \frac{Q_s}{2}\left[T_w\sqrt{\frac{3}{\sigma}(s_w + s_{vo})} - 1\right] \qquad \text{TURBULENT} \qquad (5a)$$

$$Q_e - Q_r = \frac{C_1}{C_2}\, T_w\left[\frac{Q_s{}^2}{Re_+}(s_w + s_{vo})\right]^{1/3} - \frac{Q_s}{2} \qquad \text{LAMINAR} \qquad (5b)$$

where s_w is the jet centerline arc length from the nozzle exit to the wall and the attachment parameter T_w is defined by eq (6).

$$T_w \equiv \tanh\left(\frac{\sigma n_w}{s_w + s_{vo}}\right) \qquad \text{TURBULENT} \qquad (6a)$$

$$T_w \equiv \tanh\left[C_2 n_w\left(\frac{Re_+ Q_s}{s_w + s_{vo}}\right)^{2/3}\right] \qquad \text{LAMINAR} \qquad (6b)$$

where n_w is the distance from the jet centerline to the attachment streamline evaluated at the arc distance s_w and is a function of the attachment angle, θ. The unknowns in eq (5) and (6) are the distances n_w, s_{vo}, and s_w.

2.3 Jet Deflection Equation

The equation for the jet deflection angle β is obtained by combining the continuity, Bernoulli, and momentum equations in the interaction region and assuming that the supply and control flows interact without losses. Assuming that the width of the supply jet b_+' is constant in the interaction region, then from continuity, the jet velocity u_s' is constant, and by Bernoulli's equation the supply jet pressure p_s' throughout the interaction is also constant. The control pressure p_{av}' and p_i', producing forces acting normal to the supply jet, and the control momenta, $\rho' u_c'^2 b_c$, acting in the y direction, cause the jet to deflect through an angle β, as shown in figure 1b. The force balance equation in the longitudinal (x) direction is

$$(p_{av}' - p_i')b_c' \tan\beta + p_s' b_+' - p_s' b_+' \cos\beta = \rho' u_s'^2 b_+' \cos\beta - \rho' u_s'^2 b_+'$$

Normalizing with $p_+' b_+'$ $(= \rho' Q_+'^2/2b_+')$ and rearranging gives

$$(p_{av} - p_i)b_c \tan\beta + (p_s + 2Q_s{}^2) = (p_s + 2Q_s{}^2)\cos\beta \qquad (7a)$$

By introducing the transverse forces F_a and F_i, made up by summing the control momenta $2Q_c^2/b_c$ and the y components of the pressure forces, such that

$$F = pb_c + \frac{2Q_c^2}{b_c}$$

the normalized equation for the transverse direction becomes

$$(F_a - F_i) = (p_s + 2Q_s^2) \sin \beta \tag{7b}$$

Dividing eq (7b) by (7a) and assuming that

$$(p_{av} - p_i)b_c \tan \beta << (p_s + 2Q_s^2)$$

the two equations reduce to

$$\tan \beta = \frac{(F_a - F_i)}{(p_s + 2Q_s^2)} \tag{7c}$$

where

$$F_a = p_{av}b_c + \frac{2Q_{ca}^2}{b_c} \tag{7d}$$

$$F_i = p_ib_c + \frac{2Q_{ci}^2}{b_c} \tag{7e}$$

The supply jet deflection is thus dependent on the ratio of control-to-supply momenta and pressures forces. An indirect dependence on the offset D and the wall angle α, which is intuitively suspected, comes in through the dependence of the flows and interaction region pressures on these parameters.

2.4 Momentum Equation for the Attachment Point

The momentum flux J_w which strikes the wall at an angle θ and divides at the returned flow streamline n_w is the difference between the supply momentum J_+ and the momentum peeled off by the splitter J_{sp} (see fig. 2). Assuming negligible pressure forces, the momentum flux balance equation at the attachment point is

$$J_w \cos \theta = J_{downstream} - J_{upstream}$$

or

$$\left[u_s^2 - \int_{-\infty}^{n_{sp}} u^2 dn \bigg|_{s=s_{sp}}\right] \cos \theta = \left[\int_{n_{sp}}^{n_w} u^2 dn - \int_{n_w}^{\infty} u^2 dn\right]_{s=s_w} \tag{8}$$

The distances n_{sp} and n_w are measured from the jet centerline arc to the splitter and returned flow streamline at the respective jet arc lengths s_{sp} and s_w (fig. 2 and 3). The first integral on the right in eq (8) can be written as

$$\int_{n_{sp}}^{n_w} u^2 dn \bigg|_{s=s_w} = \left[\int_{n_{sp}}^{0} u^2 dn + \int_{0}^{n_w} u^2 dn\right]_{s=s_w}$$

and since the momentum between any two lines of constant similarity parameter is conserved

$$\int_{n_{sp}}^{0} u^2 dn \bigg|_{s=s_w} = \int_{n_{sp}}^{0} u^2 dn \bigg|_{s=s_{sp}}$$

Note that $\sigma(h_{sp}/s)$ is constant so that n_{sp} has different values at $s = s_w$ and $s = s_{sp}$.

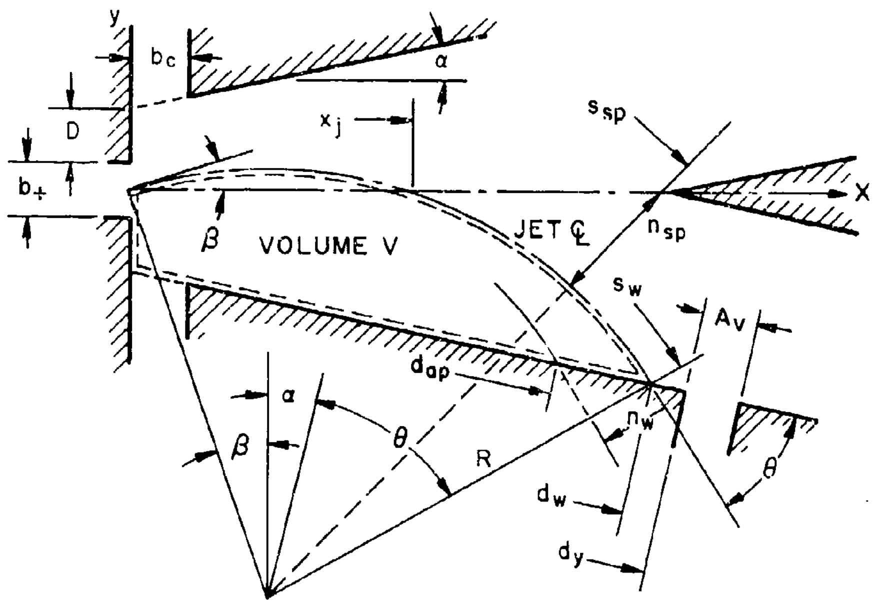

Figure 3. Basic geometry

Using the velocity profile, eq (3) and (4), and defining

$$T_{sp} \equiv \tanh\left(\frac{\sigma n_{sp}}{s_{sp} + s_{vo}}\right) \qquad \text{TURBULENT} \qquad (9a)$$

$$T_{sp} \equiv \tanh n_{sp} C_2 \left(\frac{Re_+ Q_s}{s_{sp} + s_{vo}}\right)^{2/3} \qquad \text{LAMINAR} \qquad (9b)$$

and noting the definition of T_w from eq (6a) and (6b), the momentum flux equation degenerates to

$$\left(\frac{1}{3} T_{sp}^3 - T_{sp} + \frac{2}{3}\right) \cos \theta = \frac{1}{3} T_{sp}^3 - T_{sp} - \frac{2}{3} + 2T_w - \frac{2}{3} T_w^3 \qquad (10)$$

The root of the cubic equation in T_w (eq 10) applicable to the attachment point is

$$T_w = 2 \cos\left(\frac{\pi - \cos^{-1}(\lambda/2)}{3}\right) \qquad (11a)$$

where

$$\lambda = 1 + \frac{3}{2} T_{sp} - \frac{1}{2} T_{sp}^3 + \left(1 - \frac{3}{2} T_{sp} + \frac{1}{2} T_{sp}^3\right) \cos \theta \qquad (11b)$$

The unknowns in eq (11) are n_w, n_{sp}, s_w, s_{sp}, and s_{vo}. Except for the jet virtual origin distance s_{vo}, the unknowns are determined through the geometric relationships with the jet position in the amplifier.

2.5 Upstream Location of Supply Apparent Source, s_{vo}

The previous equations involving the velocity profile, eq (2), contain the apparent source distance, s_{vo}. To determine this value, the velocity profile, eq (2), is equated to one-half the supply nozzle flow. Evaluating at s = 0 results in the expression for s_{vo}.

$$\frac{u_s b}{2} = \int_0^\infty u dn \Big|_{s=0} = \frac{k_1}{k_2}\Big|_{s=0} \qquad (13)$$

and

$$s_{vo} = \frac{\sigma}{3} \qquad \text{TURBULENT} \qquad (14a)$$

$$s_{vo} = Re_+ Q_s \left(\frac{C_2}{2C_1}\right)^3 \qquad \text{LAMINAR} \qquad (14b)$$

2.6 Momentum Flux Equations for Jet Curvature, R

An arc of a circle is assumed for the attached jet centerline curvature (fig. 1 and 3). This has recently been experimentally verified for various offsets and control flows (aspect ratio = 6, turbulent jet) by Wada and Shimizu.[2] The jet centerline radius of curvature is the ratio of jet momentum flux to the pressure difference across it, $\Delta p_b = p_i - p_b$ so that:

$$R = \frac{2Q_s^{\,2}}{\Delta p_b} \quad \text{or} \quad \Delta p_b = \frac{2Q_s^{\,2}}{R} \qquad (15)$$

While the radius of curvature of the jet can be written in terms of geometry, both Δp_b and Q_s in eq (15) depend on the bubble pressure p_b and the opposite-side pressure p_i.

Up to this point, the difference between this model and previous ones (Epstein[4] and Lush,[6] for example) is that this model takes into account the variation in flows caused by changes in the exit pressures and an interaction with the splitter. Because we are trying to describe the two-sided jet-attachment device, the pressure p_i on the opposite side of the jet is not assumed to be zero gage. This additional unknown requires another equation, which is described in the following section.

2.7 Vortex Equation for the Bubble Pressure, p_b

The attachment bubble pressure is obtained by postulating a forced vortex in the bubble. For simplicity and convenience, it is assumed that (fig. 4):

(1) The pressure distribution is given by the differential equation $\frac{1}{r}\frac{dp}{dr} = 2\omega^2$
(where ω is the angular velocity of the bubble vortex).
(2) The driving velocity at the edge of the vortex is the entrainment streamline velocity, u_e, evaluated at $s_e = s_w/2$ (fig. 4) and the pressure on the streamline is p_e.
(3) The attachment bubble pressure p_b is the integrated average of the vortex pressure distribution resulting in

$$p_b = -\frac{1}{2} u_e^{\,2} + p_e \qquad (16)$$

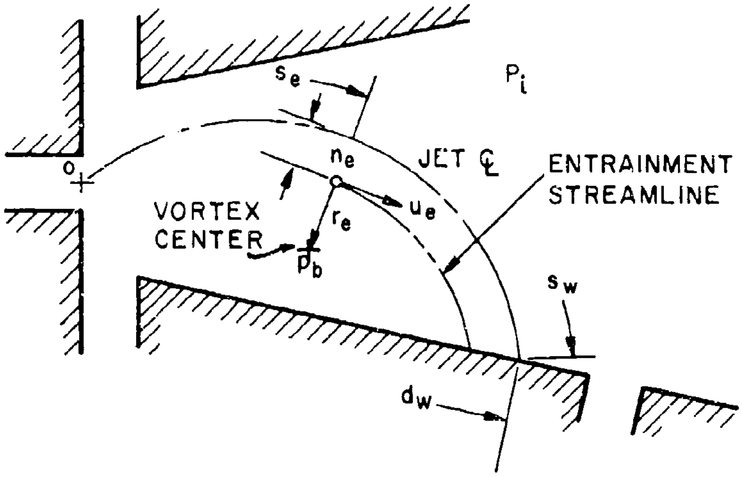

Figure 4. Bubble vortex

2.8 Vortex Driving Velocity, u_e

The vortex driving velocity u_e is obtained from the velocity profile evaluated at the downstream distance s_e and cross-stream distance n_e. The distance s_w, and hence s_e, is related to the geometry, and the distance n_e is determined by integrating the velocity profile, eq (2), between $n = 0$ and $n = n_e$ and equating the flow through one-half the supply nozzle which results in

$$n_e = \frac{1}{k_2} \tanh^{-1}\left(\frac{Q_s}{k_1}\right)\bigg|_{s=s_e} \tag{17}$$

Substituting eq (17) into the velocity equation (eq 2) gives the vortex driving velocity as

$$u_e = \frac{3}{2} Q_s \sqrt{\frac{\sigma}{3(s_e + s_{vo})}} \left[1 - \frac{\sigma}{3(s_e + s_{vo})}\right] \quad \text{TURBULENT} \tag{18a}$$

$$u_e = C_1 Q_s \left(\frac{Re_+ Q_s}{s_e + s_{vo}}\right)^{1/3} \left[1 - \left(\frac{C_2}{2C_1}\right)^2 \frac{Re_+ Q_s}{s_e + s_{vo}}\right]^{2/3} \quad \text{LAMINAR} \tag{18b}$$

Note that eq (18) is not accurate near the supply nozzle exit since the entrainment velocities are not monotonically decreasing functions of s_e because the model does not use a jet potential core region. Both the turbulent and the laminar entrainment streamline velocities increase to a maximum and then decrease for increasing values of s_e in the model; whereas, physically, the velocity on the entrainment streamline is highest near the nozzle exit and decreases as the downstream distance increases.

Rather than use eq (18) in the region where u_e is inaccurate, a cubic distribution correction is assumed for the initial downstream distances to insure that the entrainment velocity monotonically decreases from the supply nozzle velocity u_s. The cubic velocity distribution for u_e is matched to the distribution of eq (18) at the distance s_{em} associated with the maximum velocity u_{em}. With the derivatives of eq (18) set equal to zero, the maximum u_e and its location are determined.

$$\left.\begin{aligned} u_{em} &= 1/\sqrt{3} \\ s_{em} &= 2\sigma/3 \end{aligned}\right\} \text{TURBULENT} \qquad (19a)$$

$$\left.\begin{aligned} u_{em} &= \frac{C_1}{\sqrt{3}}\left(\frac{2C_1}{C_3} - \frac{1}{3}\right)Q_s \\ s_{em} &= \left(\frac{C_2}{2C_1}\right)^3 Re_+ Q_s(\sqrt{27} - 1) \end{aligned}\right\} \text{LAMINAR} \qquad (19b)$$

The cubic function for $s_e < s_{em}$ is

$$u_e = m_1 s_e^3 + m_2 s_e^2 + m_3 s_e + m_4 \qquad (20)$$

with the conditions

$$u_e = u_s \quad \text{at } s_e = 0$$

$$\frac{du_e}{ds_e} = 0 \quad \text{at } s_e = 0$$

$$u_e = u_{em} \quad \text{at } s_e = s_{em}$$

$$\frac{du_e}{ds_e} = 0 \quad \text{at } s_e = s_{em}$$

Solving for the coefficients (and noting that $u_s = Q_s$ in the normalized form)

$$m_1 = \frac{2(Q_s - u_{em})}{s_{em}^3} \qquad (21a)$$

$$m_2 = -\frac{3}{2} m_1 s_{em} \qquad (21b)$$

$$m_3 = 0 \qquad (21c)$$

$$m_4 = Q_s \qquad (21d)$$

Equations (18) are used for $s_e > s_{em}$ and eq (20) and (21) for $s_e \leq s_{em}$.

2.9 Geometric Relations

The geometric relations presented in the following sections are shown in figure 3. The attachment wall offset distance D is measured from the edge of the supply nozzle to the beginning of the attachment wall plane, and the attachment wall angle α is measured with respect to the x-axis or axis of symmetry. The vent distance d_v, the jet centerline attachment point d_w, and the attachment point d_{ap} are all measured from the exit plane of the supply nozzle along the attachment wall. The jet radius of curvature is R. The centerline arc distance s_w is measured from the exit plane to the jet centerline attachment point. The deflection angle of the jet is β. Both the jet centerline and attachment streamline (extended to the wall) intersect the wall at an angle θ.

From the geometry, the jet radius of curvature is

$$R = \frac{(D + 0.5)\cos \alpha}{\cos (\alpha + \beta) - \cos \theta} \tag{22}$$

the jet arc length is

$$s_w = R(\alpha + \beta + \theta) \tag{23}$$

and the jet centerline attachment distance is

$$d_w = R[\sin (\alpha + \beta) + \sin \theta] - (D + 0.5)\sin \alpha \tag{24}$$

The attachment point is located by the intersection of the returned flow streamline with the wall. Assuming a right-triangle relationship with the jet centerline point d_w and attachment angle θ, the attachment point is

$$d_{ap} = d_w - n_w/\sin \theta \tag{25}$$

When the jet centerline intersects the amplifier axis downstream of the splitter, it can be considered as a switch, since more than half of the jet flow is on the opposite side. The intersection of the jet centerline and the amplifier axis is

$$x_j = 2R \sin \beta \tag{26}$$

2.10 Attachment Bubble Volume under Jet Centerline, V

The volume V (per unit depth) of the attachment bubble is bounded by the supply nozzle exit plane, the attachment wall plane, and the jet centerline so that

$$V = 0.5R^2\{\alpha + \beta + \theta - 0.5[\sin 2(\alpha + \beta) + \sin 2\theta]\} + [R \sin(\alpha + \beta) - 0.5(D + 0.5) \sin \alpha](D + 0.5)\cos \alpha \tag{27}$$

Because of the formulation of the present model, there is the possibility that the jet centerline may intersect the opposite wall. Rather than reformulate all of the equations to match the conditions imposed by the solid opposite wall, it is assumed that the jet curvature remains constant even though it would pass through the wall. From figure 5, the jet flow corresponding to this situation is assumed to be equivalent to the jet radius of curvature R deflected through an angle and striking the opposite wall at the point IN. The jet centerline extends through the wall and intersects the wall again at point OUT. In reality, however, the jet flow is parallel to the wall along the chord length IN-OUT. At OUT, the jet flow separates from the wall and continues in the direction of the jet centerline. Any resultant wall pressure is assumed equivalent to the pressure required to change the circular path of the jet to a straight path. The pressures p_b and p_i are affected indirectly only by the different volume used in the calculations.

The attachment bubble is reduced by the area of the segment of circle defined by the points IN and OUT. Figure 5 shows the x-y coordinate system with the origin at the center of the supply nozzle exit. The x-coordinates of the points IN and OUT are obtained from the solution of the equations for the opposite wall

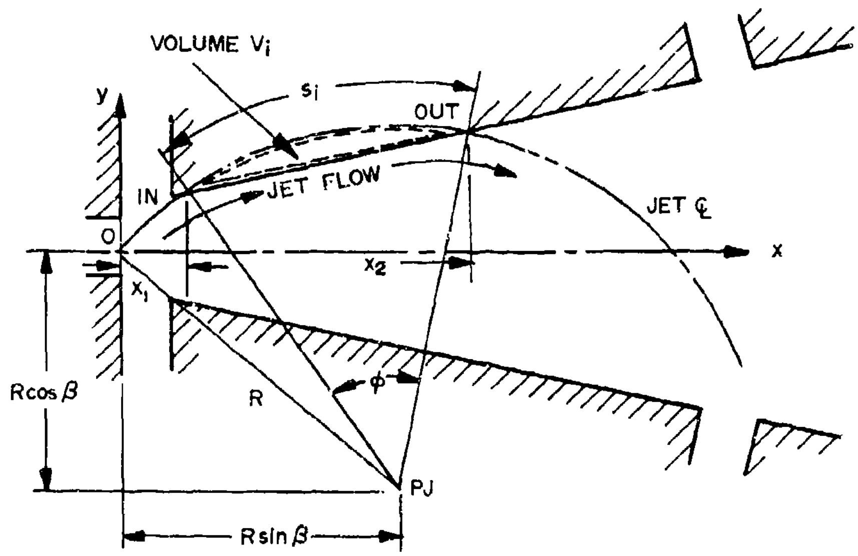

Figure 5. Jet touching opposite wall

$$y = x \tan \alpha + D + 0.5 \tag{28}$$

and the jet centerline circle

$$R^2 = (x - R \sin \beta)^2 + (y + R \cos \beta)^2 \tag{29}$$

which gives

$$x_1 = - BW - \sqrt{BW^2 - CW} \tag{30}$$

$$x_2 = - BW + \sqrt{BW^2 - CW} \tag{31}$$

where

$$BW = \cos^2 \alpha \; [(D + 0.5 + \cos \beta)\tan \alpha - R\sin \beta] \tag{32}$$

$$CW = [(D + 0.5)\cos \alpha]^2 + 2(D + 0.5)R\cos \alpha \cos \beta \tag{33}$$

The angle ϕ subtending the arc s_i, between IN and OUT is given by

$$\phi = \sin^{-1}\left[\sin \beta - \frac{x_1}{R}\right] + \sin^{-1}\left[\frac{x_2}{R} - \sin \beta\right] \tag{34}$$

The area V_i to be subtracted from eq (27) is

$$V_i = 0.5R^2(\phi - \sin \phi) \tag{35}$$

so that the geometric equation for the attachment bubble volume enclosed by the jet centerline V_b is

$$V_b = V - V_i \tag{36}$$

2.11 Lumped Parameter Line Equations

As mentioned previously, the supply, control, vent, and output channels are characterized as lumped-parameter lines. These line equations are derived by integrating Euler's equation along a streamtube assuming one-dimensional, incompressible flow with no body forces. Along some streamtube z, the normalized integrated form of Euler's equation between two points z_1 and z_2 is

$$2\int_{z_1}^{z_2} \frac{\partial u}{\partial t}\, dz + u_2{}^2 - u_1{}^2 = p_1 - p_2 \tag{37}$$

Since $u(z,t) = Q(t)/A(z)$, the equation can be written as

$$2\,\frac{dQ}{dt}\int_{z_1}^{z_2} \frac{dz}{A(z)} + u_2{}^2 - u_1{}^2 = p_1 - p_2 \tag{38}$$

The integral is the inductance of the line, but for convenience, it is multiplied by two, so that the inductance parameter L is defined as

$$L \equiv 2\int_{z_1}^{z_2} \frac{dz}{A(z)} \tag{39}$$

The inductance parameter depends on the geometry of the line between any point z_1 chosen as the input (or beginning) of the line and the point z_2, which terminates inside the amplifier.

The remaining terms in eq (38) can be arranged so that the designer/experimenter has a choice of using either the static or the total pressure as the input pressure signal. For practical application, losses must be accounted for. They are included in Euler's equation by using the discharge coefficient, $c_d = Q_{actual}/Q_{ideal}$. In terms of the total input pressure, $p_{t_1} = p_1 + u_1^2$, and the actual flow Q, the line equation is

$$\frac{L}{c_d}\frac{dQ}{dt} + KQ|Q| = p_{t1} - p_2 \tag{40}$$

where the resistance parameter K is defined as

$$K \equiv \frac{1}{c_d{}^2 A_2{}^2} \tag{41}$$

where A_2 = area (per unit depth, normalized) at station z_2. Using $Q|Q|$ in the expression allows flow in a line to be in either direction. In terms of static pressure input p_1, the line equation is

$$\frac{L}{c_d}\frac{dQ}{dt} + \left(K - \frac{1}{A_1{}^2}\right)Q|Q| = p_1 - p_2 \tag{42}$$

Of course when $(c_d A_2/A_1)^2 << 1$ and $p_1 \approx p_{t1}$, the two forms of the line equations become equivalent. The discharge coefficient relationship is of the form

$$c_d = (1 - a_1/\sqrt{Re})(1 - a_2/\sqrt{Re})$$

where a_1 and a_2 are determined from the solution of the Karman-Pohlhausen momentum integral equations for a particular nozzle.

2.11.1 Supply Equation

The normalized supply total pressure is equal to one, as is the normalized supply nozzle width, so that the supply resistance parameter $K_s = 1/c_{ds}^2$. The supply line equation is then

$$\frac{L_s}{c_{ds}} \frac{dQ_s}{dt} + K_s Q_s^2 = 1 - p_s \tag{43}$$

Note that no reverse flow is anticipated.

Equation (43) couples the supply flow to any changes in the interaction region pressures.

2.11.2 Control Equations

The control line equations are, from eq (40),

$$\frac{L_c}{c_{dc}} \frac{dQ_{ca}}{dt} + K_{ca} Q_{ca} |Q_{ca}| = p_{ca} - p_{av} \tag{44a}$$

$$\frac{L_c}{c_{dc}} \frac{dQ_{ci}}{dt} + K_{ci} Q_{ci} |Q_{ci}| = p_{ci} - p_i \tag{44b}$$

The total pressures p_{ca}, p_{ci} are the input forcing functions for the entire system of equations. For symmetrical devices, the inductance parameter L_c and the discharge coefficient c_{dc} relationship are the same for both control lines. The resistance for the controls is based on the distance between the downstream edge of the control and the edge of the jet. The edge of the jet is determined by considering the jet to be of constant width after emerging from the supply nozzle until it passes the downstream edge of the controls. At the downstream edge of the control (fig. 6, distance b_c), the amplifier has a half-width B. The effective opening (through which flow may pass) of the attached-side control is

$$A_{ca} = (B - 0.5) + \Delta y_c \tag{45a}$$

where Δy_c is the distance between the amplifier axis and the jet centerline. By convention, Δy_c is positive when $\beta > 0$. The opening for the opposite control is

$$A_{ci} = (B - 0.5) - \Delta y_c \tag{45b}$$

The resistance of the controls is therefore

$$K_{ca,ci} = 1/A_{ca,ci}^2 = 1/(B - 0.5 \pm \Delta y_c)^2 \tag{46}$$

The expression for Δy_c is obtained from the equation of the jet centerline whose radius is R and whose center is at the point PJ (fig. 6). The circular path passes through the point $PC(b_c, \Delta y_c)$ so that, from the equation of a circle

$$R^2 = (b_c - R\sin\beta)^2 + (\Delta y_c + R\cos\beta)^2$$

and so

$$\Delta y_c = -R\cos\beta + (R^2\cos^2\beta - b_c^2 + 2b_c R\sin\beta)^{1/2} \tag{47}$$

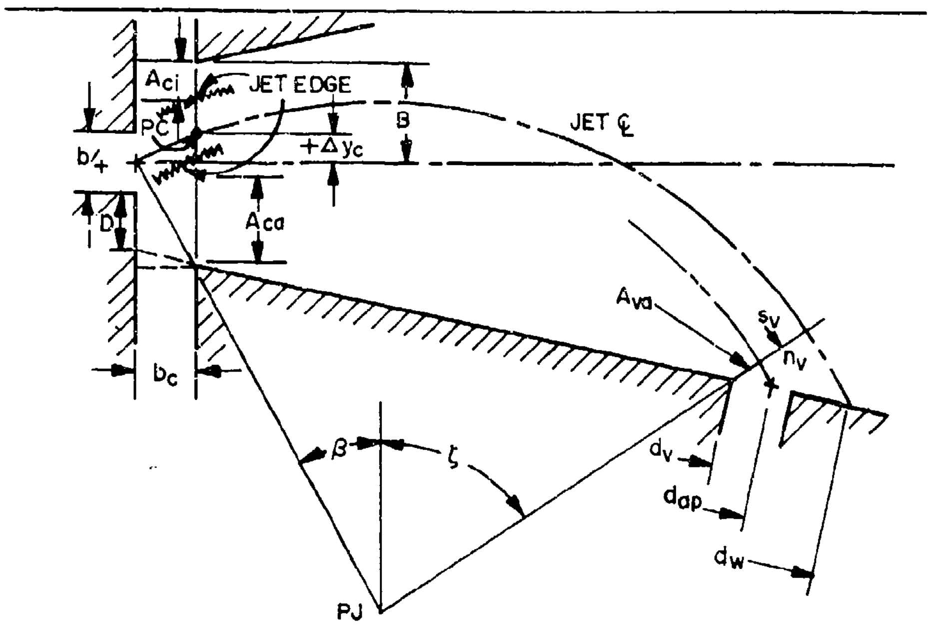

Figure 6. Control and vent restriction distances

Note, however, that Δy_c can be positive or negative, and so $K_c \to \infty$ if $\Delta y_c = (B - 0.5)$. To eliminate such large values of K_c, since physically the controls can never be completely blocked by a transverse fluid stream, a maximum value is assumed for practical purposes. Despite the fact that the jet width is assumed constant when calculating $A_{ca,ci}$, eq (45), the maximum value for resistance K_{cmax} is based on a jet spread of 0.14 rad (8 deg). Then, even though the edge of the jet touches the wall and geometrically blocks the control, we assume that the control flow sees an effective orifice whose width is equal to the amount that the jet has spread at the downstream edge of the control. The maximum control resistance based on this minimum opening A_{cmin} is

$$K_{cmax} = 1/A_{cmin}^{2} = 1/[b_c \tan(0.14)]^2 \tag{48}$$

When the jet spacing is greater than the nozzle width b_c, a minimum resistance is reached and is defined as

$$K_{cmin} \quad 1/[b_c c_{dc}]^2 \tag{49}$$

The discharge coefficient is set equal to unity when the effective resistance is due to jet modulation, since it is assumed that when one side of a restriction is a fluid-fluid interface at high velocity, the effect of the solid-wall boundary layer is negated, and so there is essentially no viscous retardation on the average.

2.11.3 Vent Equations

The attached-side vent pressure difference is the ambient pressure p_{va} minus the bubble pressure p_b, and the opposite-side vent pressure difference is the ambient pressure p_{vi} minus the opposite-side pressure

p_i. In most cases, the vent ambient pressures are equal, so that $p_{va} = p_{vi} = p_v$. The vent line equations are, from eq (40),

$$L_{va} \frac{dQ_{va}}{dt} + K_{va} Q_{va} |Q_{va}| = p_v - p_b \tag{50a}$$

$$L_{vi} \frac{dQ_{vi}}{dt} + K_{vi} Q_{vi} |Q_{vi}| = p_v - p_i \tag{50b}$$

On the attached side, the effective vent width for the inductive and resistive parameters is based on the distance between the upstream edge of the vent and the relative position of the returned flow streamline. If the jet attachment point is upstream of the vent, the vent flow into the bubble is zero. As the attachment point sweeps past the vent, the effective opening increases from zero to the physical width of the vent channel. The attached-side vent inductive parameter L_{va} is variable to compensate in some measure for the reduction in vent area caused by the jet flow that is directed into the vent as the jet centerline is passing the vent. The minimum resistance K_{vmin} based on the maximum vent opening is then

$$K_{vmin} = 1/W_v^2 \tag{51}$$

On the opposite side, the vent is never covered by the jet (at least for the anticipated geometries considered here); therefore, $K_{vi} = K_{vmin}$ = constant. On the attached side, however, resistance values greater than K_{vmin} occur depending on the effective vent opening A_{va} (fig. 6). This distance is measured along the jet radial line passing through the upstream corner of the vent and extending to the attachment streamline. The arc length s_v of the jet centerline to the radial line passing through the vent corner is

$$s_v = R(\beta + \zeta) \tag{52}$$

where

$$\zeta = \tan^{-1}\left[\frac{d_v \cos \alpha - R \cos \beta}{R \cos \beta - (D + 0.5) - s_v \sin \alpha}\right] \tag{53}$$

At the arc distance s_v, the distance from the jet centerline to the attachment streamline is n_v. The expression for n_v is obtained by using the similarity properties for the jet solution. Since the similarity parameter is constant for a particular streamline, in this case, the returned flow streamline, its value is obtained at the jet centerline attachment point, $s = s_w$. The value of the similarity parameters for the attachment streamline are

$$\eta = \frac{\sigma n_w}{s_w + s_{vo}} \qquad \text{TURBULENT} \tag{54a}$$

$$\xi = C_2 n_w \left(\frac{Re_+ Q_s}{s_w + s_{vo}}\right)^{2/3} \qquad \text{LAMINAR} \tag{54b}$$

where the n_w's are given by eq (12). The distance n_v is obtained by combining eq (52) through (54) yielding

$$n_v = n_w\left(\frac{s_v + s_{vo}}{s_w + s_{vo}}\right) \qquad \text{TURBULENT} \tag{55a}$$

$$n_v = n_w\left(\frac{s_v + s_{vo}}{s_w + s_{vo}}\right)^{2/3} \qquad \text{LAMINAR} \tag{55b}$$

The effective restriction for vent flow is therefore

$$A_v = R - n_v - \frac{d_v \cos\alpha - R \sin\beta}{\sin\zeta} \tag{56}$$

and the resistance parameter for the vent is

$$K_v = 1/A_v{}^2 \tag{57}$$

when $A_v < W_v$. The area A_v is then also used in the inductive parameter L_{va} when the jet is sweeping by the vent.

2.11.4 Output Equations

The equations for the output lines are, from eq (40),

$$L_{oa}\frac{dQ_{oa}}{dt} + K_{oa}Q_{oa}|Q_{oa}| = (p_i + p_{da}) - p_{oa} \tag{58a}$$

$$L_{oi}\frac{dQ_{oi}}{dt} + K_{oi}Q_{oi}|Q_{oi}| = (p_i + p_{di}) - p_{oi} \tag{58b}$$

The pressures p_{oa} and p_{oi} are the static pressures at the external measuring point of the output lines. The total pressures $(p_i + p_{da})$ and $(p_i + p_{di})$ provide the internal driving force to the output lines. Since the active output line is for the most part separated from the bubble by the jet, the static pressure at the entrance to it, as well as to the inactive output line, is p_i.

The dynamic pressures p_{da} and p_{di} are determined from the momentum flux impinging on the output receivers of area $W_{oa} = W_{oi} = W_o$. The momentum flux impinging on the active output line is that which is flowing downstream from the attachment point. Averaging the momentum over the entrance area of the output line yields the dynamic pressure such that:

$$p_{da} = \frac{1}{2}\,\frac{J_{downstream}}{W_o} \tag{59}$$

where $J_{downstream}$ is given by eq (8). Equation (8) also includes the momentum peeled off by the splitter. Averaging this momentum over the inactive output line opening gives the dynamic pressure p_{di} impinging on that output as

$$p_{di} = \frac{1}{2}\,\frac{J_{splitter}}{W_o} \tag{60}$$

The dynamic pressures can be expressed in terms of the attachment point parameters T_{sp} and T_w (eq 6, 9, 10, and 11).

$$p_{da} = 0.75Q_s{}^2[T_{sp} + T_w - (T_{sp}{}^3 + T_w{}^3)/3]/W_o \tag{61a}$$

$$p_{di} = 0.75Q_s{}^2[2/3 - T_{sp} + T_{sp}{}^3/3]/W_o \tag{61b}$$

The resistance parameters of the outputs are constant at $K_{oa} = K_{oi} = K_o = 1/W_o^2$. The inductive parameters of all lines are a function of their shape and are obtained by using eq (39).

Various expressions have been developed herein to describe the bistable amplifier model. The line equations couple the conditions external to the amplifier to the internal conditions; however, the coupling of the equations in the internal region of the amplifier depends on the pressure level term p_e (eq 16). A constant control volume around the entire amplifier is used to calculate the pressure p_e, which is continuously adjusted so that the net flow is zero. Thus, since the relationships for all the flows into the unit are known as functions of the respective pressure differences, there is always one value of p_e (and hence of all the other pressures) that will satisfy continuity at any given time. By calculating all the line flows (as determined by the respective pressures) and summing them, a non-zero result may occur. If it does, then p_e is adjusted so that the net flow is zero.

3. METHOD OF SOLUTION

The geometric and flow equations (1 through 61) are solved, simultaneously where necessary, on a digital computer. The programming language is the Digital Simulation Language DSL/90,[12] a sub-language based on FORTRAN IV with a large built-in library of internal functions and subroutines which allow simple commands to be used when solving complex differential and implicit equations. Of the several integration routines available in DSL/90, the technique chosen was Milne, a fifth-order, predictor-corrector routine with variable time-step size.

Equations (4), (43), (44), (50), and (58) are integrated in time. Arbitrary, but reasonable, values are assinged as initial conditions for the integrals. The program then takes the assigned values of the program, geometric and fluid constants and parameters, and in conjunction with the governing set of equations, relaxes the problem variables to the actual steady-state values. These values then constitute the initial conditions for the transient response of the bistable amplifier to an arbitrary input pressure signal which is impressed after the initial relaxation time.

The program listings are presented in appendix A. The program names and variables are defined there as are the specific instructions for program start-up. In the calculation of the incremental change in pressure level, an iterative procedure at each time step is specified during the simultaneous solution calculation of the entire set of equations. Subsequent iterations are based on the new pressure level. This iteration at each time step used excessive machine time and so was discarded in favor of the following alternate method. The sum of the flows calculated from the various equations was generally non-zero. Instead of iterating to find a true value of p_e at a particular time step, a change was calculated simply as a function of the net flow. The error incurred was less than 2 percent, overall.

---

[12] Syn, W.M. and Wyman, D.G., "Digital Simulation Language User's Guide," IBM Systems Development Division, San Jose, California, TR 02.355, 01 July 1965.

4. RESULTS

Three levels of complexity are presented. First, the theory in its simplest form is used to predict the switching dynamics of fluid amplifiers for the case where splitter and output effects are negligible. An intermediate formulation is used to predict the switch time (time to reach the splitter) of the jet when the splitter and output effects are not negligible. In this case, however, the jet remains curved towards the initial attachment wall. Finally, the most complex model is used to predict the response of an entire fluid amplifier, in which the jet is allowed to completely reattach to the opposite side by allowing a reversal in jet curvature. The physical constants for air were used. A constant value of 10 was used throughout for the spread parameter, σ.

4.1 Comparison of Turbulent Attached Jet Results with Published Data

Before initiating the Harry Diamond Laboratories (HDL) experimental effort, the simple analytical results were first compared to existing published data. These results may also be found in Goto and Drzewiecki.[9]

4.1.1 Steady-State Attached Turbulent Jet, Negligible Splitter and Output Effects (Simplest Model)

The steady-state attached jet solution considers a two-wall geometry with closed control ports. With no control flow, there is no momentum deflection of the jet and the effect of the opposite wall is minimized although not removed.[13] The essential difference between this case and the single-wall, steady-state model is that for a given supply pressure, the two-wall model has more supply flow because of the negative pressure in the interaction region. Figure 7 shows the agreement between the predicted results and the experimental data of Kimura and Mitsuoka[3] for the attachment distance d_{ap} versus offset D for a wall angle of 0.262 rad (15 deg), with aspect ratio (AR) of about 3.3.

Lush[8] (fig. VIII, p. 36) gives steady-state experimental data for turbulent jet attachment distance versus offset for open control ports. The analytical results for Lush's geometry were obtained by opening both controls to zero (gage) input pressure at time zero and allowing the jet to reach a new equilibrium position. As shown in figure 7, the agreement between the present theory and Lush's experimental data is good for the given range, $0 \leq D \leq 1.0$, for a wall angle of 0.262 rad (15 deg) and AR = 1.0.

4.1.2 Switch Time of the Turbulent Attached Jet with Negligible Splitter and Output Effects

The experimental switch time data of Johnston[14] and Lush[8] are compared here with theoretical results. Johnston's data was obtained on two test models that had no splitter or side wall vents. One unit had a length of nine nozzle widths, the other 17. The dimensions are given by Johnston[14] and also by Goto and Drzewiecki[9] and are shown in figures 8 and 9.

---

[13]Perry, C.C., "Two-Dimensional Jet Attachment," Advances in Fluidics, Proc. ASME Fluidics Symposium, Chicago, May 1967.

[14]Johnston, R.P., "Dynamic Studies of Turbulent Reattachment Fluid Amplifiers," Master's Thesis, University of Pittsburgh, School of Engineering and Mines, 1963.

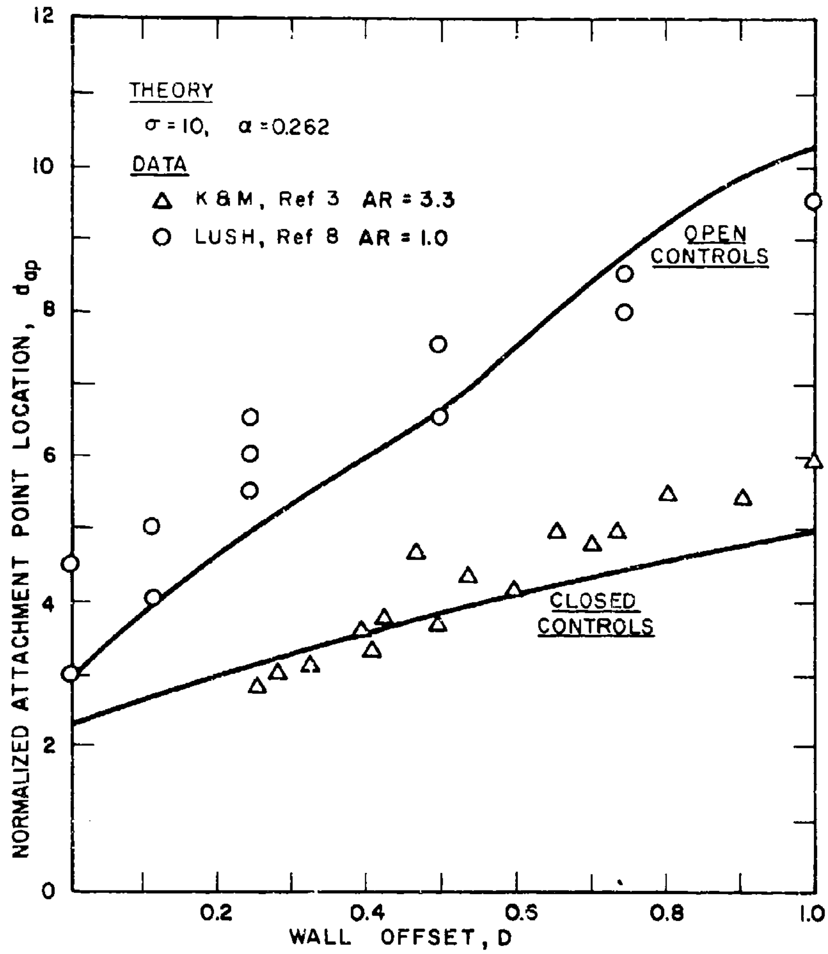

Figure 7. Turbulent attachment distance versus offset

The time it takes for the jet centerline to intersect the unit axis at 9.0 or 17.0 nozzle widths, the ends of the units, is considered to be the switching time. Switching times were calculated using a signal that reached the selected pressure after a 200- μs ramp to duplicate Johnston's input signal. Figures 8 and 9 show the experimental data and the analytical results of switching time versus the various final input pressure amplitudes. For each case, both the analytical curve for the attachment point reaching the end of the wall (separation) and the jet centerline intersecting the axis at the end of the model are shown.

The agreement between theoretical switching time and experimental data is better for the short-wall model (fig. 8) than for the long-wall model (fig. 9). In the latter case, at the lower values of input pressure, the jet radius of cu vature is quite large, so that when the

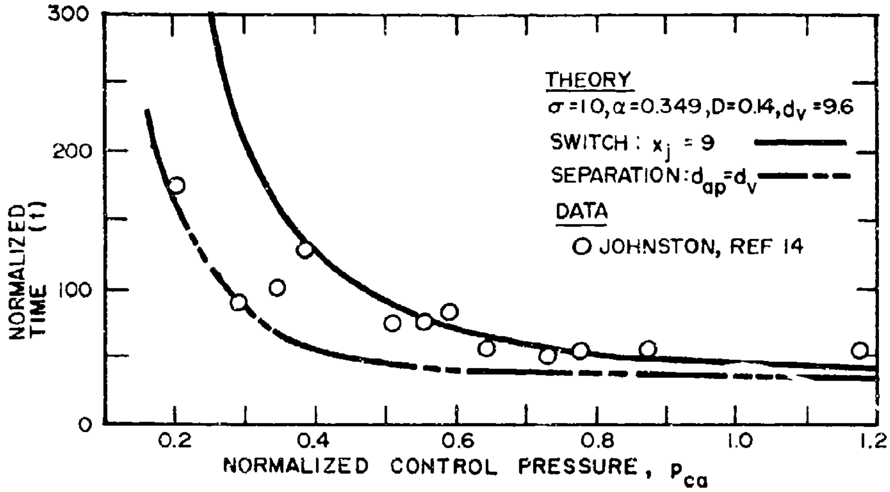

Figure 8. Turbulent jet switching time versus control pressure, 0.2 ms ramp input, Johnston's short wall data

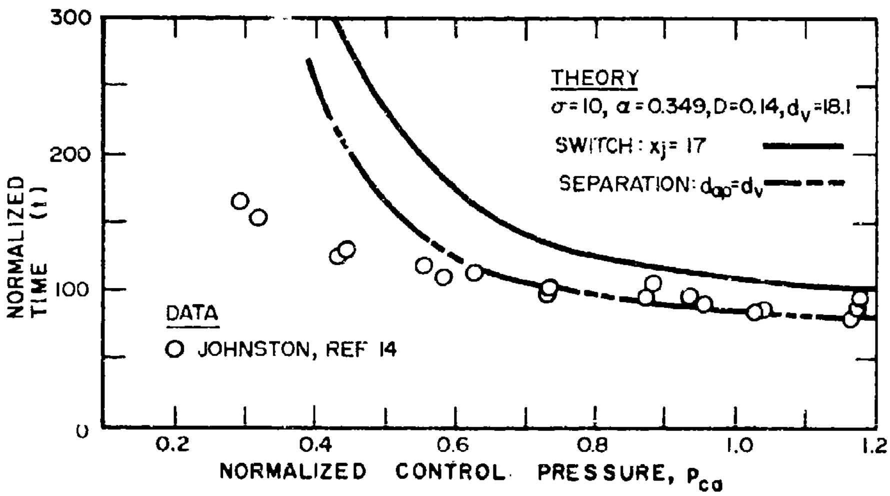

Figure 9. Turbulent jet switching time versus control pressure, 0.2 ms ramp input, Johnston's long wall data

centerline intersects the axis at 17 nozzle widths, a major portion of the jet and the vortex are outside the model geometry. The analytical model no longer applies when the jet is outside the geometry, since one no longer expects the jet to curve. The effect of such a lack of curvature would be an increase in vent flow and, therefore, a decrease in switch time. In general, the agreement for both geometries is fairly good, since the line dimensions and signal characteristics were estimated from photographs presented by Johnston.[14]

Lush's test model had a splitter at 20 nozzle widths downstream (to minimize splitter effects) and a 0.262-radian (15-deg) wall angle. The supply and control nozzles were 2.54 cm (1.0 in.) with an aspect ratio of one. Offset was 0.482, d_v was 13.04, and A_v was 2.2. The other dimensions were estimated and, in nozzle widths, are: the supply chamber length, 5; width, 3; control chamber length, 3; width, 1; and vent length, 3. Details of his geometry are given by Lush.[8] In his model, the controls were initially open to atmosphere. His 10- to 20-ms pressure rise-time input signal (Lush,[8] p. 76) is represented in this model by a 20-ms ramp to a final pressure amplitude. The experimental switch time was measured from the beginning of the pressure-flow rise in the control chamber to the time the jet reached the end of the opposite wall. Using the initial simple theory, the analytical switch time was started at the same point but ended when the jet centerline intersected the amplifier axis at $x_{sp} = 20$ (the splitter distance). Figure 10 shows the experimental and analytical results of switching time versus final control-pressure amplitude. As is shown, the theory agrees well with the data.

No comparison has been made with Muller's data,[15] since there was not sufficient information about his splitter shape and location, output line dimensions, and input measuring locations. His device was a symmetrical, low-offset device, so it was unfortunate that comparisons could not be made.

4.2 HDL Experimental Apparatus and Methods

The HDL experimental program was initiated after obtaining good agreement between the initial simple analysis and existing published data. The purpose of the experimental program was to compare the analyses of the simple model, the intermediate model, and the most complex model to data of amplifier characteristics such as steady-state recovery, switching characteristics, and actual amplifier response time.

4.2.1 Instrumentation

Figure 11 is a diagram and figure 12 a photograph of the HDL test set-up. A hot-film anemometer probe was flush-mounted in the test model cover plate and located at a given point on the geometric axis of the device. As the jet switched, the maximum, or centerline velocity passed that point, and the anemometer registered a maximum voltage. The response of the constant-temperature, hot-film system was greater than 20 kHz; however, the output signal was electronically filtered to pass only 5 kHz. The control signal was initiated by an electromechanical solenoid valve upstream from the control port connection to the test model. The control flow entered the device perpendicular to the

---

[15] Muller, H.R., "Wall Reattachment Device with Pulsed Control Flow," Proc. 2nd Fluid Amplification Symposium, HDL, Vol. 1, May 1964.

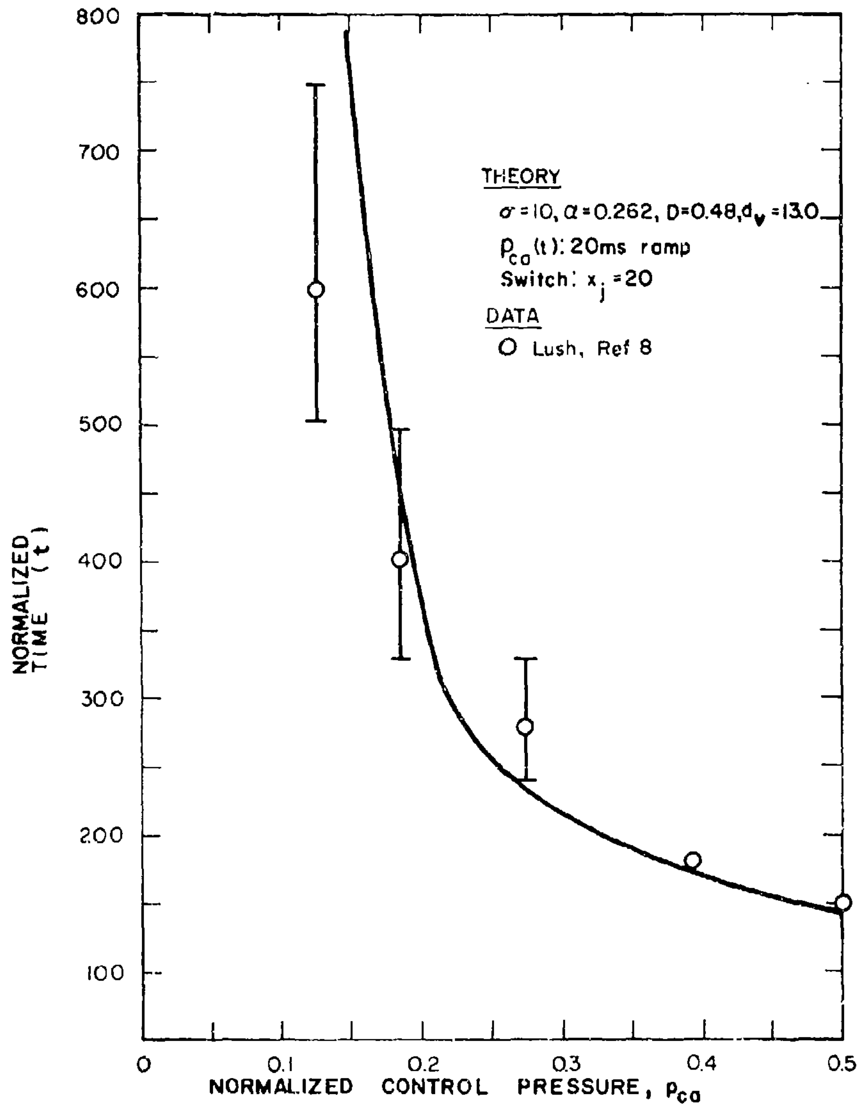

Figure 10. Turbulent jet switching time versus control pressure, 20 ms ramp input, Lush's data

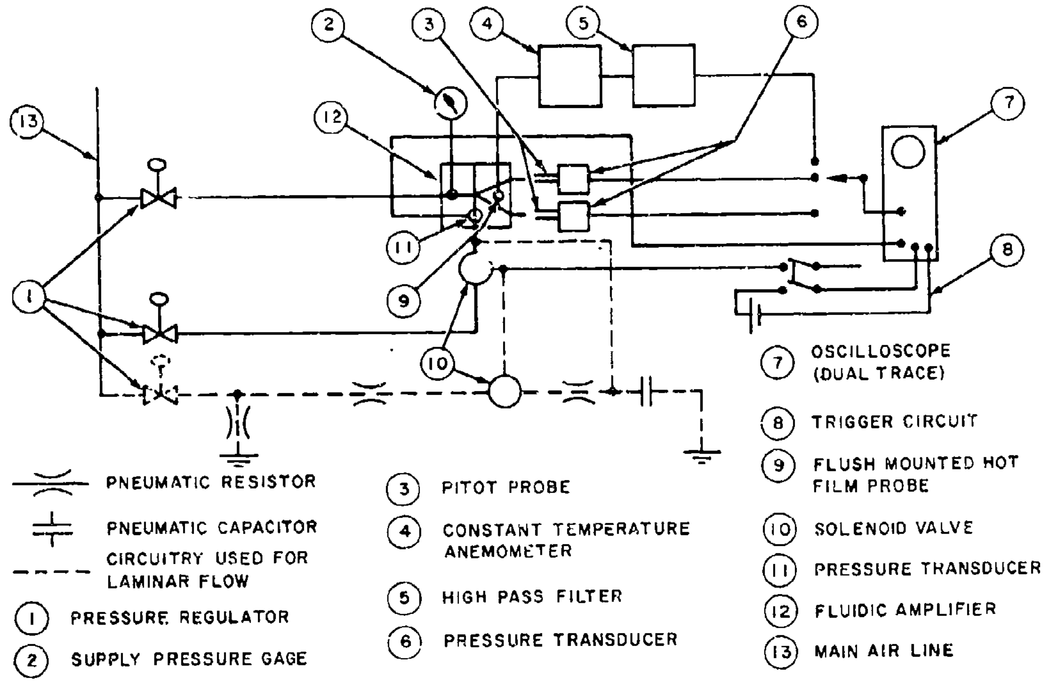

Figure 11. HDL test setup.

cover plate and impinged directly on a strain-gage type pressure transducer mounted in the bottom of the control channel. The transducer measured the total pressure of the impinging flow. (This transducer measurement of total pressure was verified by actual total pressure probe measurements.) The response of the pressure measuring system was less than 0.05 ms and was neglected, since the rise time of the input signal was around 1.5 ms. Output total pressures were measured with a pitot probe which had a 3-mm diameter and was 2 cm long. It was fitted directly into a strain-gage type pressure transducer. The response was estimated at over 4 kHz. The control signal and the hot-film output were monitored simultaneously on a dual-trace oscilloscope to determine the time history of the control signal and the time to move the jet centerline past the hot-film. Steady state control flows into the amplifier configuration were measured with laminar-flow meters.

4.2.2 Experimental Models

Table I lists the dimensions of the three large configurations tested. Except for the offsets D, control line areas W_c, and the depths, the models had the same plan-view geometry. The splitter, when used, was a plexiglas wedge with an included angle of 0.418 rad (24 deg) that could be located at any desired position in the configuration. The location of the splitter was chosen as 10 nozzle widths downstream of the power nozzle, since splitters in most actual fluidic devices are located at about that distance.

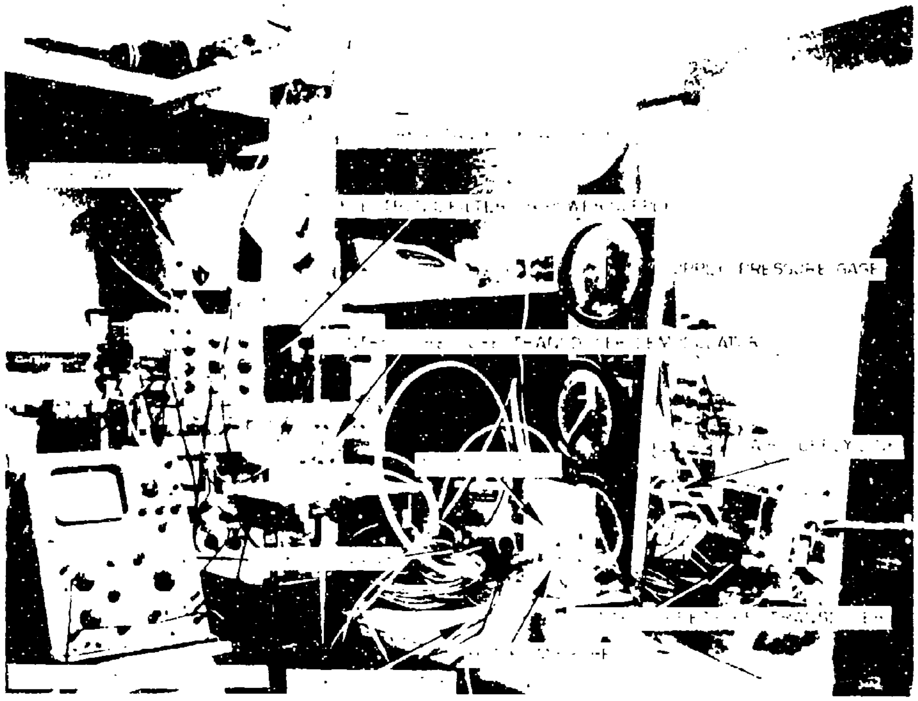

Figure 12. Photograph of experimental apparatus.

Table I. Test Model Dimensions

Model 1 (Aluminum)		Model 2 and 3 (Plastic)	
$b_+' = 2.1$ mm		$b_+' = 2.0$ mm	
$b_c' = 2.1$ mm	$b_c = 1.0$	$b_c' = 2.0$ mm	$b_c = 1.0$
$\alpha = 0.209$ rad (12 deg)		$\alpha = 0.209$ rad	
$D' = 1.9$ mm	$D = 0.9$	$D' = 1.0$ mm	$D = 0.5$
$d_v' = 18.0$ mm	$d_v = 8.6$	$d_v' = 18.0$ mm	$d_v = 9.0$
$h' = 6$ mm	AR = 3	$h' = 4$ mm	AR = 2

LINE SIZES

Supply: length = 30 mm; width, $W' = 10$ mm	Vent: length = 20 mm; width, $W_v' = 4$ mm
Control: length = 20 mm; width, $W_c' = 4$ mm (20 mm for Model 3)	Output: length = 56 mm; width, $W_o' = 7$ mm

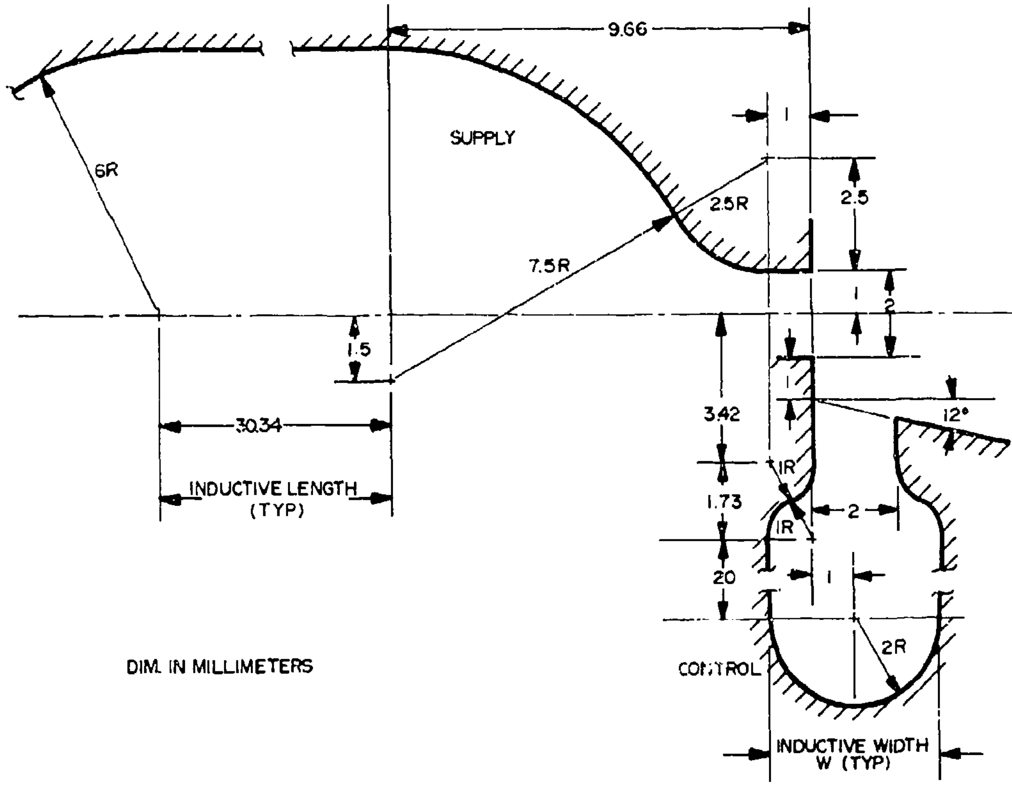

Figure 13. Supply and control geometry for Model 2.

The pattern for experimental Models 1 and 2 was programmed and then drawn by a digital computer in conjunction with a Cal-Comp plotter using the AUTOSKEM program shown in appendix B. The plotter also provided a twice size (2:1) cut-and-strip negative of the device. Using a photoetching process (Dycril), a template in plastic was obtained so that the models could be manufactured on a pantograph milling machine. Model 1 was milled in aluminum, and Model 2 in phenolic plastic. The control line cross sectional areas of Model 2 were later enlarged, resulting in Model 3.

4.2.3 Discharge Coefficients, c_d

Instead of solving for the discharge coefficient c_d (sec 2.11), the discharge characteristics of the supply and control nozzles in this study were determined experimentally. As previously noted, the nozzles for all models were the same width. The supply nozzles had a contraction ratio (cross sectional area of line to orifice area) for Models 1 and 2 of six and a contraction length ratio (length over which contraction occurs to orifice area) of five. The control nozzles for Models 1 and 2 had a contraction ratio of two and a contraction length ratio of 0.875. Modifying the Model 2 control line resulted in a contraction ratio of 10 (Model 3). Figure 13 shows the supply and control geometry for Model 2, which is representative of all the models (except for D).

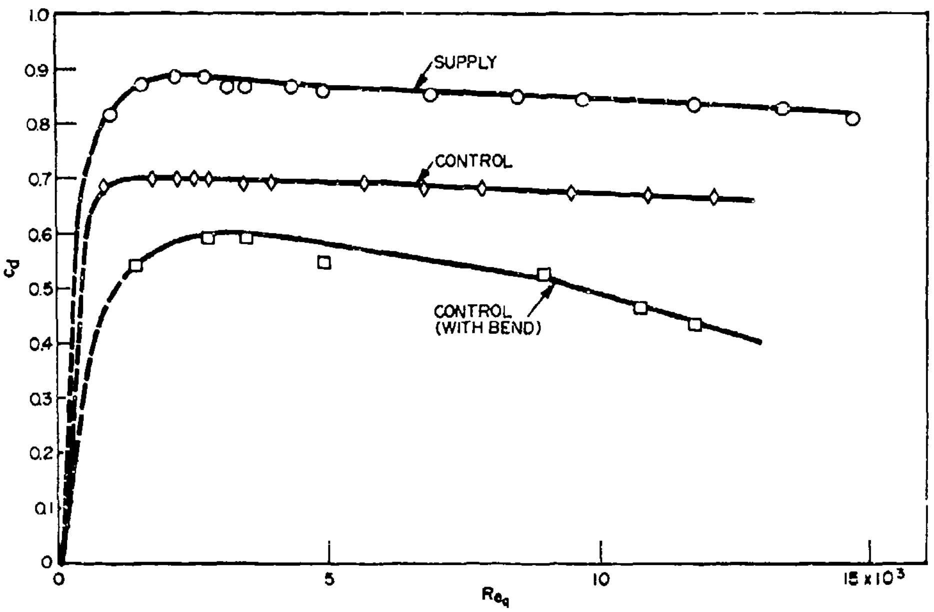

Figure 14. Discharge coefficients versus Reynolds number.

Figure 14 shows the discharge coefficients c_d as a function of Reynolds number, $Q'/h'\nu'$ (based on nozzle width and actual flow), for the test models. The supply c_{ds}'s were the same for all models within the experimental error. Two discharge curves were obtained for the control nozzles. The upper curve for the control discharge coefficient c_{dc} is the actual c_{dc} curve for the nozzles. The lower curve is actually a line-loss coefficient, because the point of measurement upstream from the nozzle included an elbow fitting as well as the control nozzle. The curve is presented because some switch time experiments (Model 1 without the splitter) had used that measurement point to monitor the control input signal.

For simplicity in the analysis, the supply discharge coefficient was assumed constant because the variation of supply flow during a switching calculation was small compared to the variation of c_{ds} with Re. The turbulent switching experiments were run at Reynolds numbers of $Re_+ = 15,000$ to 18,000, and the laminar at $Re_+ = 1000$. Supply discharge coefficients of $c_{ds} = 0.85$ and 0.80, respectively, were used. Control coefficients for the analysis were based on a linear approximation to the data, because the control flow and hence, control Reynolds number varied significantly during the time-dependent calculations.

4.3 Comparison of Turbulent Attached Jet Results with HDL Data

4.3.1 Switching Time of the Turbulent Attached Jet with Negligible Splitter and Output Effects

Model 1 was used to obtain the time response of a turbulent, attached jet without splitter effects. The supply pressure was fixed at 7.5 kPa (1.09 psig). The input-pressure signal was a ramp to a preselected level and was applied to the attached-side control. The ramp duration from the initial pressure, p_{av}, to the final input value p_{ca} varied from between 1 and 2 ms. In the analytical computations, the input ramp rise-time was fixed at 1.5 ms.

The hot-film probe was located at 10 nozzle widths downstream. The time at which the probe registered the maximum signal was used as the experimental switch time. The time at which the jet centerline intersected the amplifier axis at 10 nozzle widths was used as the analytical switch time. Control pressure versus switch time data was collected for two conditions of inactive control port loading: blocked, and open to ambient pressure. Figure 15 shows the data with the inactive control blocked ($Q_{ci} = 0$), and the agreement is excellent over the entire range of input control pressures. Figure 16 shows the data where the inactive control was open to ambient pressure ($Q_{ci} \neq 0$). The agreement is fairly good over the range, but the theory slightly underestimates the switch time at the higher input pressures. As expected, both the theoretical and experimental switch times are slower if the inactive control is open rather than blocked, because there is a switch-retarding flow coming in through the inactive control, making the opposite control pressure higher.

4.3.2 Switch Time of the Turbulent Attached Jet with Splitter and Output Effects (Intermediate Model)

Experimental data were obtained on two flueric amplifiers, Models 1 and 2. Both had sharp splitters with their leading edges located at 10 nozzle widths downstream of the supply exit plane where $b_1^{\prime} = 2$ mm. The supply pressures were 10 kPa and u.6 kPa, respectively. Again, input-pressure signals consisting of 7.5-ms ramps to a final pre-selected level were used. Figures 17-20 show the comparison between theory and data. With exception of the case in figure 19, the agreement is good. No immediate explanation is offered for the discrepancy at low values of input pressure shown in figure 19.

4.3.3 Response Time of a Flueric Wall-Attachment Amplifier (Intermediate Model)

The total pressures of the outputs during switching were measured with a pitot probe located at the exit plane of the output line. Measurement of both the active and inactive outputs during switching were made, but not simultaneously. Model 3 was used in this test, with the supply pressure at 7.5 kPa. The inactive control was blocked and the input signal final amplitude was 0.25 of the supply pressure, after a 1.5-ms duration ramp.

Figure 21 shows the comparison between experiment and theory. The agreement is good in the region up to and just past the point where the jet centerline passes the splitter ($t^{\prime}_{xj=10}$); past that point, the data and theory diverge because the intermediate theory does not allow for a reversal of jet curvature. Just after the jet centerline passes the point of the splitter, the jet actually attaches to the opposite side, whereas, the intermediate model centerline attachment point continues to sweep downstream on the original attachment side.

In general, if one considers the theoretical amplifier response to be the time of intersection of the active and inactive pressure traces, then agreement with experiment is very good when compared to the rise time of the inactive output signal. Figure 21 shows that the inactive output reaches 90 percent of its final value between 5 and 5.5 ms, and the theoretical output curves intersect at about 5.5 ms.

4.3.4 Steady State Characteristics of Flueric Wall Attachment Amplifiers (Intermediate Model)

As a further test of the design utility of the analytical model, several theoretical and experimental steady state values were compared.

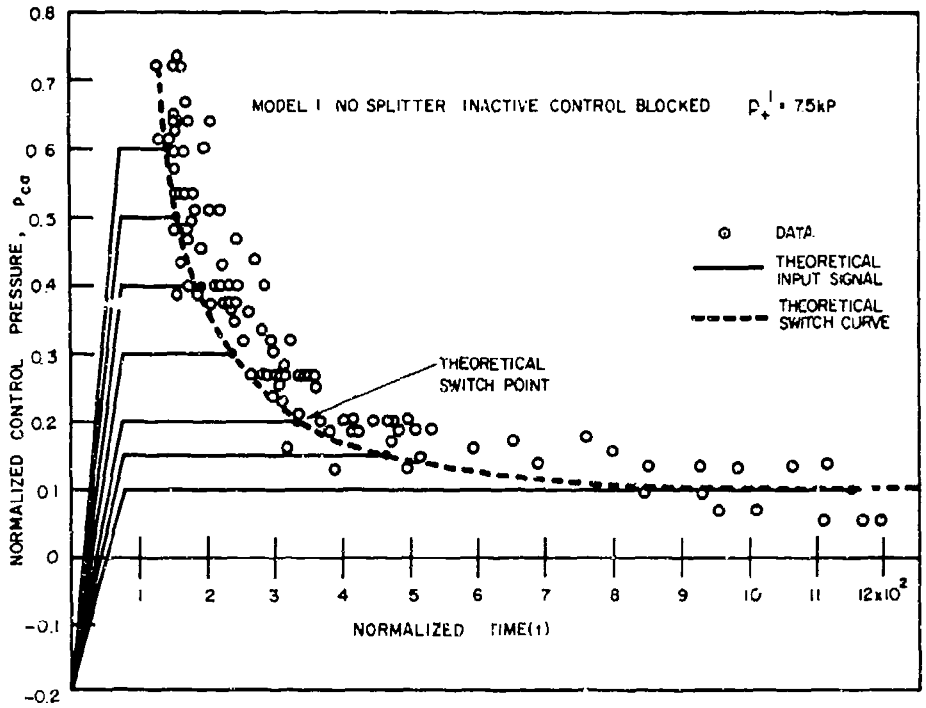

Figure 15. Control pressure amplitude versus switch time—no splitter, inactive control blocked, D = 0.9.

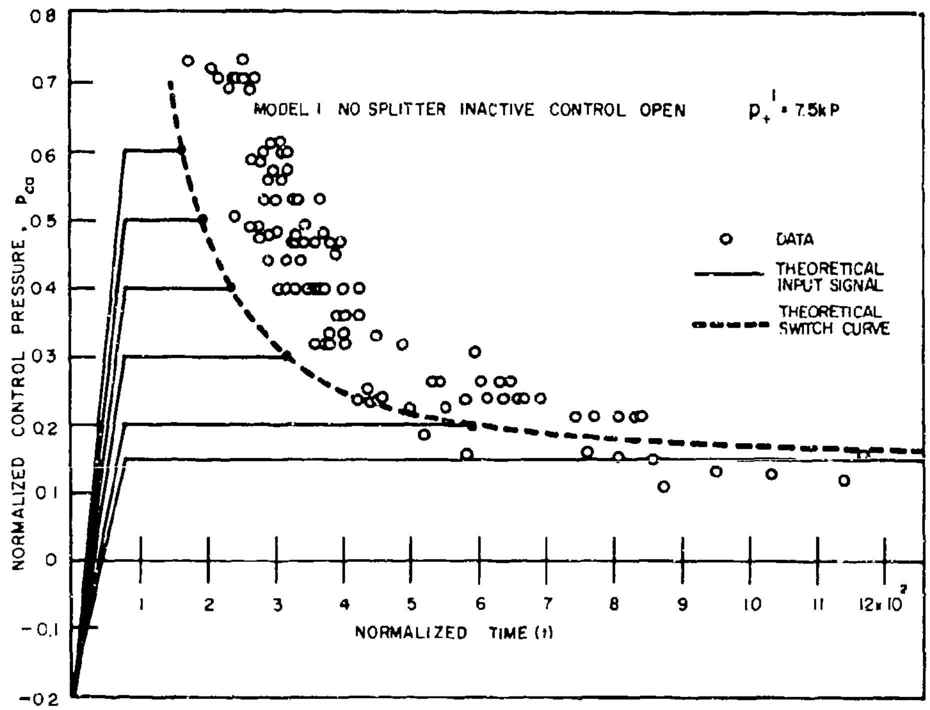

Figure 16. Control pressure amplitude versus switch time—no splitter, inactive control blocked, D = 0.9.

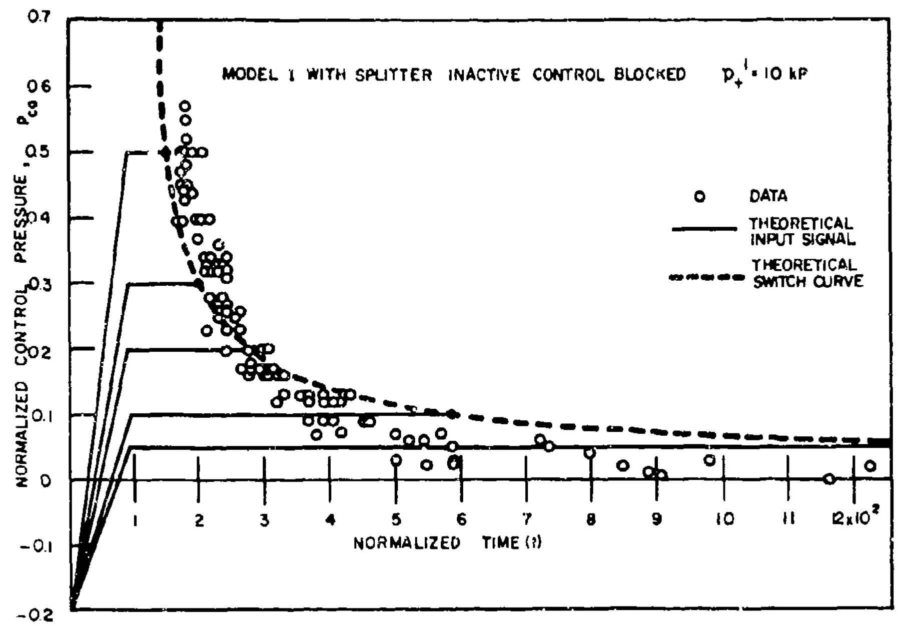

Figure 17. Control pressure amplitude versus switch time—with splitter, inactive control blocked, D = 0.9.

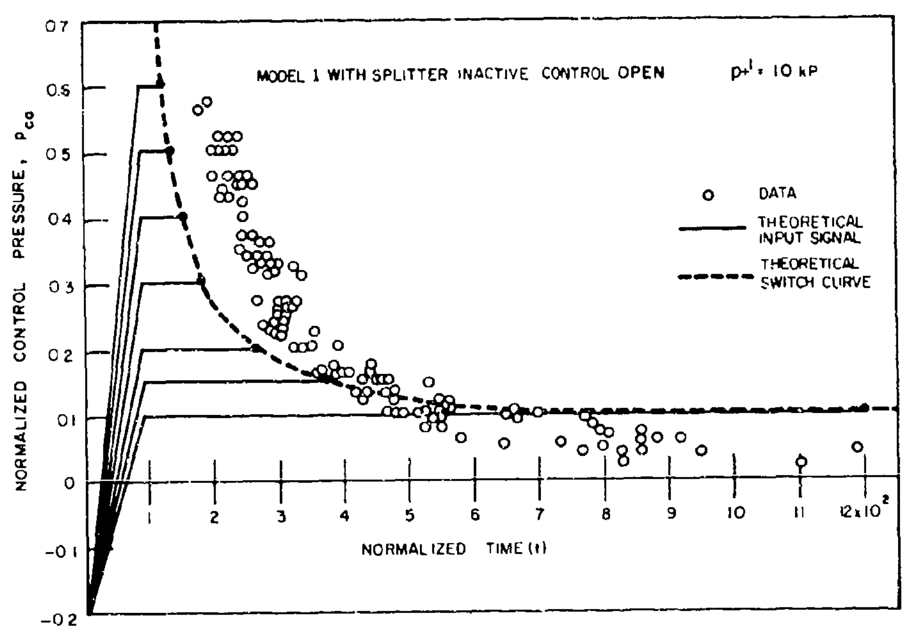

Figure 18. Control pressure amplitude versus switch time—with splitter, inactive control open, D= 0.9.

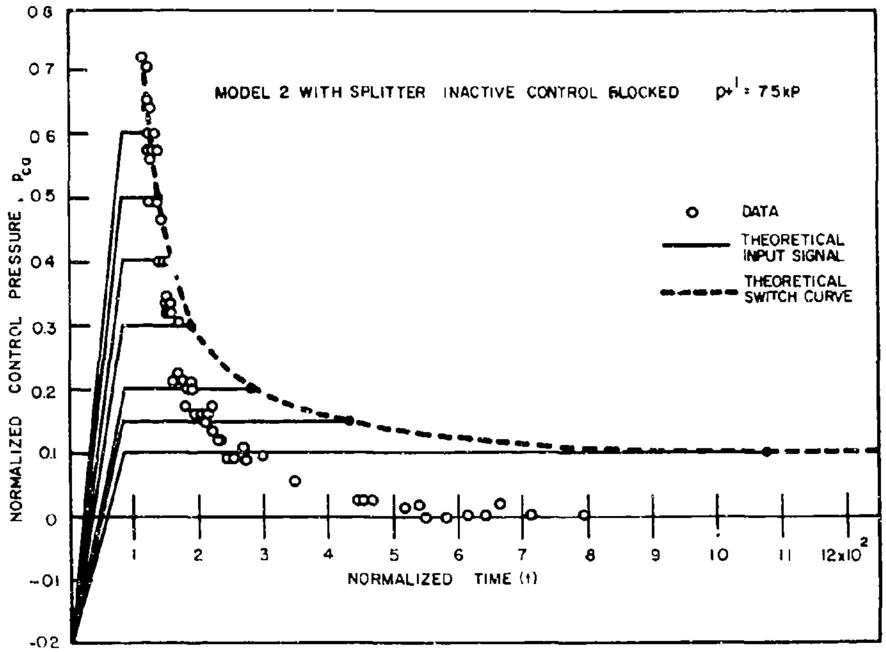

Figure 19. Control pressure amplitude versus switch time—with splitter, inactive control blocked, D = 0.5.

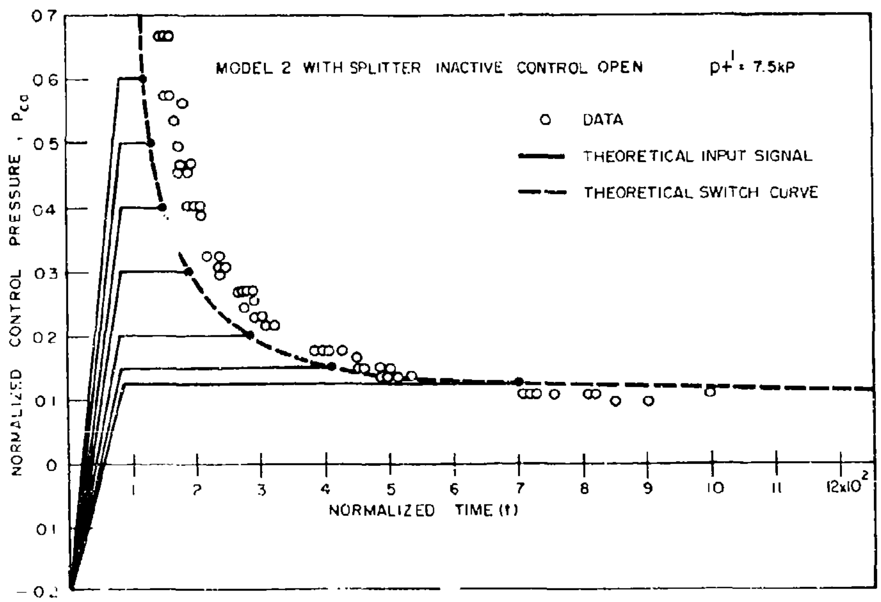

Figure 20. Control pressure amplitude versus switch time—with splitter, inactive control open, D = 0.5.

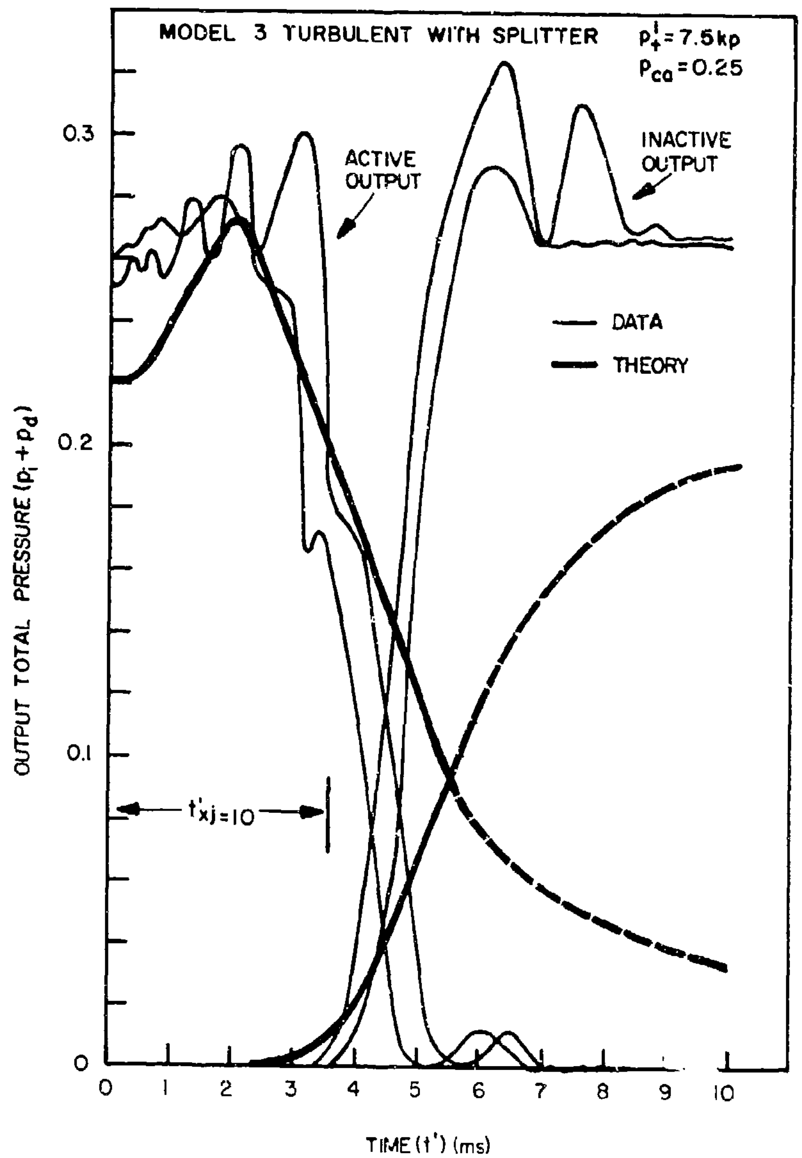

Figure 21. Transient output total pressure versus time

The control characteristics Q_c versus P_c were obtained from each side of the amplifier for both open and blocked inactive control ports. Although the characteristics for the two controls of a model were slightly different, they were averaged to maintain clarity (fig. 22 and 23). The points of comparison with theory are the pressure at zero flow and the pressure and flow at switching.

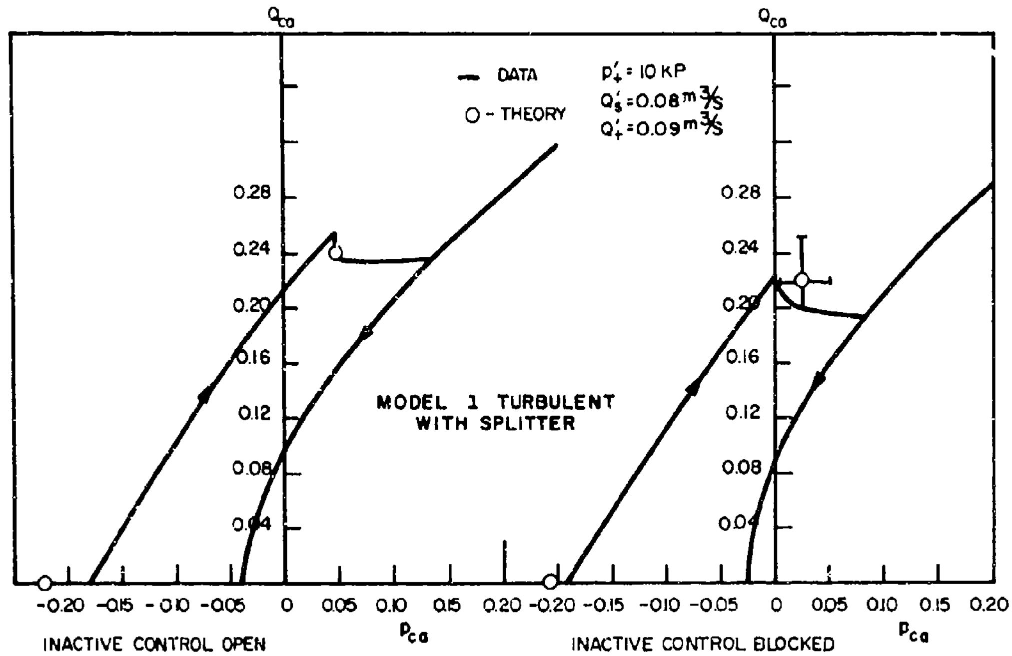

Figure 22. Control characteristics, Model 1.

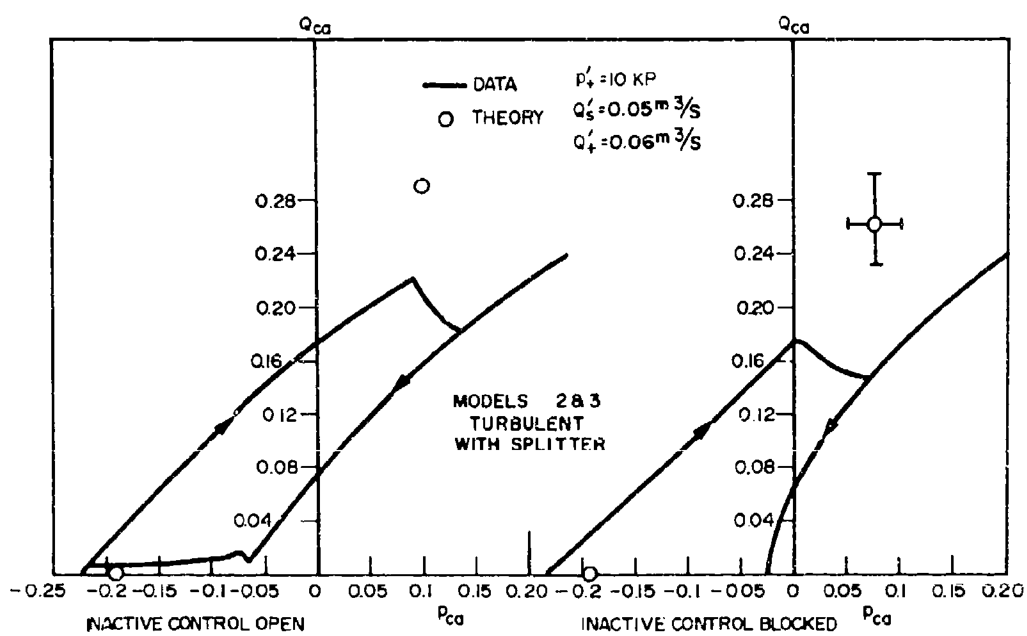

Figure 23. Control characteristics, Model 2.

The value of the initial condition of the active control exit pressure (p_{av} at $t = 0$) of the present tests corresponds to the experimental pressure at zero flow. The value of minimum pressure to switch corresponds to the experimental steady-state switch pressure. Theoretical values of minimum pressure to switch were not determined explicitly since the control pressure was pre-selected in the computer program. For this reason, a range of values for the theoretical minimum switch pressure is used for the comparison with experiments. The theoretical values shown in figures 22 and 23 show that the agreement is good.

The experimental, dynamic-pressure transfer characteristics for the active output, $p_o (= p_i + p_{da})$ versus p_{ca} are shown in figures 24 and 25. The outputs are completely open so that the output pressure is the total pressure measured with a pitot probe at the exit plane of the output lines. Because of some slight asymmetry encountered, transfer curves for both outputs of Model 1 are given, whereas a single curve is representative of measurements on either side of Model 2. The points of comparison with theory are the total pressures of the active output when the active control is blocked, open to ambient, and at the switching pressure level. The respective theoretical quantities are determined from the values of the flow out of the active output converted to a dynamic pressure when: the control input pressure level equals the control exit pressure at time zero (p_{av} at $t = 0$); the input pressure signal level is zero gage; and at the minimum switching pressure level. The comparison is made in figures 24 and 25 with the agreement being good in most respects.

The comparison of experimental and analytical steady state values associated with the characteristics curves presented above are summarized in table II, which lists their numerical values.

4.3.5 Miscellaneous Results

Since the analytical and experimental results obtained agree favorably, unverified analytical results can be presented with some measure of confidence. Results for any variable can be obtained from the computer program, but the attachment point, active-control flow, and the inactive-output flow are chosen as illustrative of the events during a switch. Figure 26 shows these variables as a function of the dimensionless time ($t = t'/t'_+$) and real time t'. The results correspond to the conditions shown in figure 19 for Model 2 with a splitter, $p'_+ = 7.5$ kPa, inactive control blocked, and p_{ca} 0.1.

The attachment point distance d_{ap} and the control flow Q_{ca} increase rapidly, until the final control pressure $p_{ca} = 0.1$ is reached at $t' =$ 1.5 ms. Note that Q_{ca} has a small overshoot. Although the control pressure is now constant, the bubble pressure is changing and the attachment point distance and control flow once again increase until the attachment point reaches the vent ($d_v = 9$). Uncovering the vent changes the control flow into the bubble so that it fluctuates while the attachment point dwells on the edge of the vent. The attachment point distance then increases again, jet switching starts, and the splitter begins to intercept flow. This is shown by the increase of the inactive output flow Q_{oi} when switching begins. The motion of the attachment point slows down on "seeing" that output's inductance. Muller[15] shows control flow overshoot and slight oscillation in much the same manner as does the present analysis.

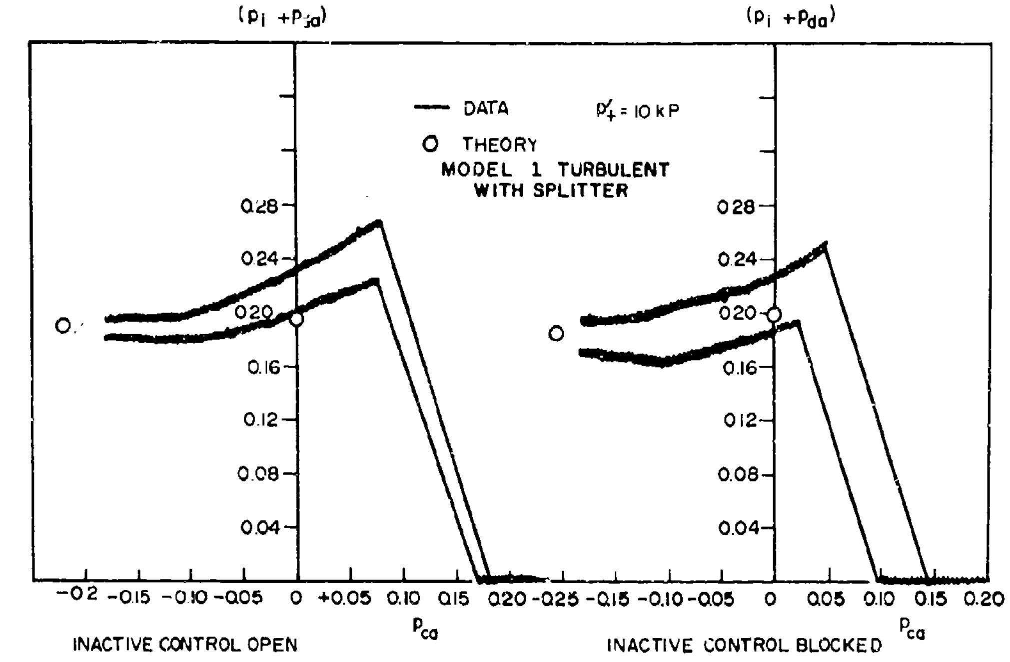

Figure 24. Transfer characteristics, Model 1.

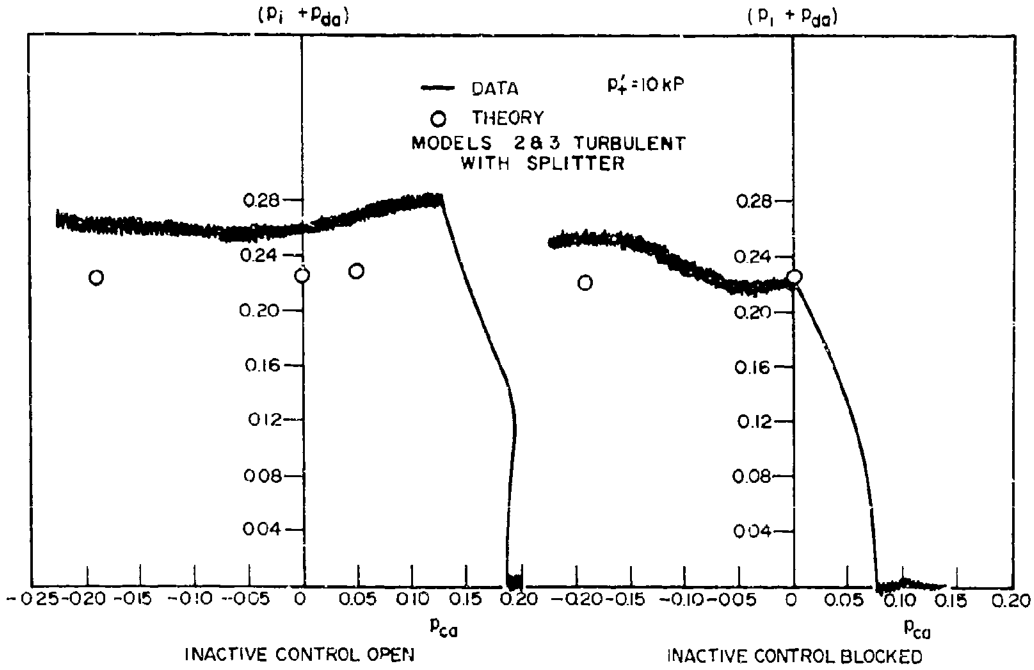

Figure 25. Transfer characteristics, Model 2.

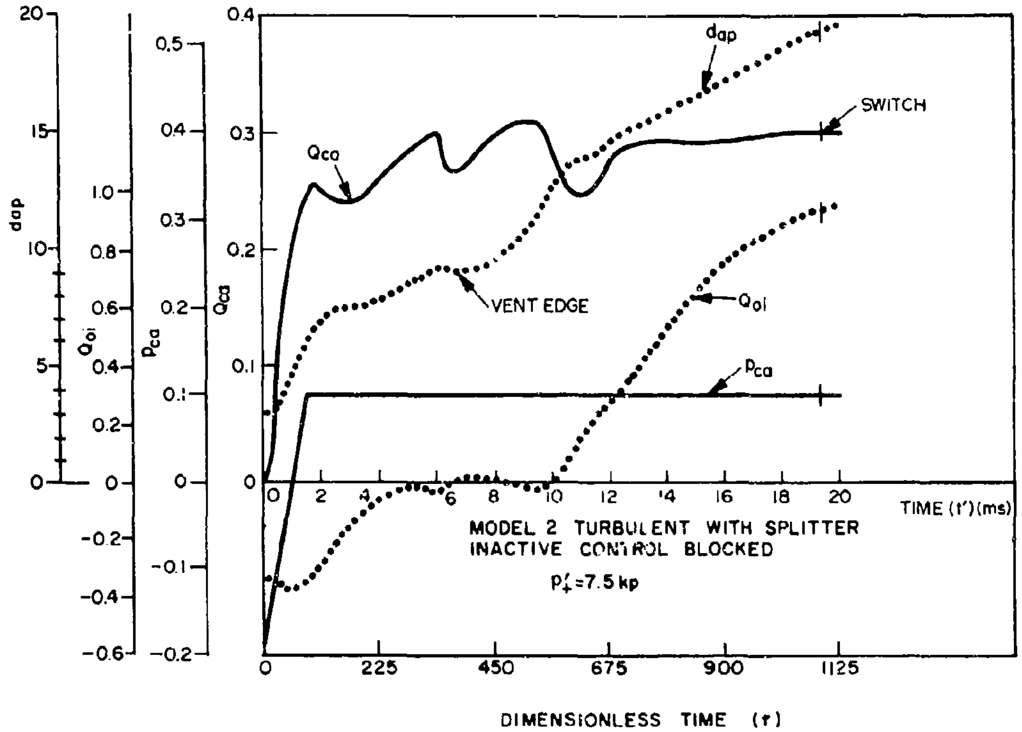

Figure 26. Analytical turbulent output variables during switching, Model 2.

Table II. Steady State Characteristics.

Active Control Condition	Inactive Control Condition	Model 1 Experiment Side 1	Model 1 Experiment Side 2	Model 1 Theory	Model 2 & 3 Experiment Side 1	Model 2 & 3 Experiment Side 2	Model 2 & 3 Theory
Steady State Dynamic Pressure Recovery ($p_i + p_{da}$)							
Blocked	Blocked	0.195	0.173	0.186	0.268	0.257	0.221
p_{ca}=0.0	Blocked	0.236	0.188	0.198	0.221	0.221	0.227
Blocked	Open p_{ci}=0	0.195	0.180	0.190	0.270	0.255	0.244
p_{ca}=0.0	Open p_{ci}=0	0.233	0.2?3	0.199	0.261	0.261	0.226
p_{ca}=0.5	Open p_{ci}=0	---	---	---	0.270	0.270	0.229
Steady State Active Control Pressure (p_{av} at $t = 0$)							
Blocked	Blocked	-0.170	-0.190	-0.208	-0.235	-0.215	-0.191
Blocked	Open p_{ci}=0	-0.170	-0.180	-0.220	-0.225	-0.200	-0.188
Minimum Active Control Pressure to Switch							
Active	Blocked	0.0	+0.01	0.0-0.05	0.0	0.0	0.05-0.10
Active	Open p_{ci}=0	+0.04	+0.05	0.05	+0.08	+0.09	0.10
Minimum Active Control Flow to Switch							
Active	Blocked	0.23	0.23	0.20-0.25	0.17	0.17	0.23-0.30
Active	Open p_{ci}=0	0.26	0.26	0.24	0.22	0.22	0.29

4.4 Comparison of Laminar Attached Jet Results with HDL Data

Model 2 was used to obtain the switch times of a laminar attached jet. The supply pressure was fixed at $p_{+}' = 0.0333$ kPa so that the Reynolds number $Re_{+} = 1000$, based on nozzle width and p_{+}'. Tests at $Re_{+} < 1000$ were not conducted because of pressure regulation difficulties at very low supply pressures. Based on the work of Comparin et al[10] and the quiet hot-film probe output, laminar flow was presumed. Low level control inputs were also difficult to regulate; therefore, the imposition of an input pressure ramp that increased to a final level (as used in the turbulent tests) was discarded. Instead the laminar input signal was adjusted so that switching occurred on a rising ramp. Because the laminar control signal was different from the turbulent signal, the presentation of the data is slightly different. For these tests, the slope of the ramp, $\Delta p/\Delta t$, is plotted against switch time. Figure 27 shows the laminar experimental results in good agreement with the theory. A single theoretical curve is given because the difference between the analytical results for open and blocked inactive controls was insignificant.

For the turbulent jet, analytical results of attachment point distance, control flow, and inactive output flow were presented as a function of time (fig. 26). Except for the attachment point distance, the same variables are shown in figure 28 for Model with a laminar jet. Since the attachment point is initially past the vent, the distance x_j (the distance from the supply exit to the intersection of the jet centerline and the geometric centerline) is shown instead. The results shown in figure 28 are for a ramp input $\Delta p_{ca}/\Delta t = 7.4 \times 10^{-4}$. The distance x_j starts from a negative value (jet deflection is slightly negative) and increases smoothly until it approaches the splitter ($x_j = 10$). The control flow Q_{ca} increases monotonically after an initial lag. From a practical viewpoint, the output flows Q_{ca} and Q_{oi} are of interest. Note that there is always some flow from the inactive output Q_{oi}, and unlike the turbulent case, there is not as large a change in either output flow with switching.

4.5 Comparison of the Switch Time of a Laminar and a Turbulent Jet

Model 2 with a splitter and the inactive control open was used to obtain laminar and turbulent analytical data. Since the intermediate theory has been shown to be valid, the analytical results for laminar and turbulent switch times can be compared. Turbulent values are taken from the data used in figure 20, but are replotted as $p_{ca} - p_{av}$ in figure 29. The theoretical input-control signals are also shown. For this com- the values of laminar data of (fig. 27) are used. From the laminar values of the slope, $\Delta p_{ramp}/\Delta t$, corresponding to the slope of the turbulent control ramp inputs, the laminar switching times are determined. Comparison of the laminar and turbulent switching curves on figure 29 shows that the normalized laminar switching rate is faster than the turbulent. Figure 29 also shows representative real-time values for switching. Laminar real times range from 15 to 22 ms, whereas the turbulent values range from 3 to 18 ms.

4.6 Response of a Flueric Wall-Attachment Amplifier (Most Complex Model)

By allowing the jet to reattach to the opposite wall after separating from the initial wall in the analytical model, the complete time

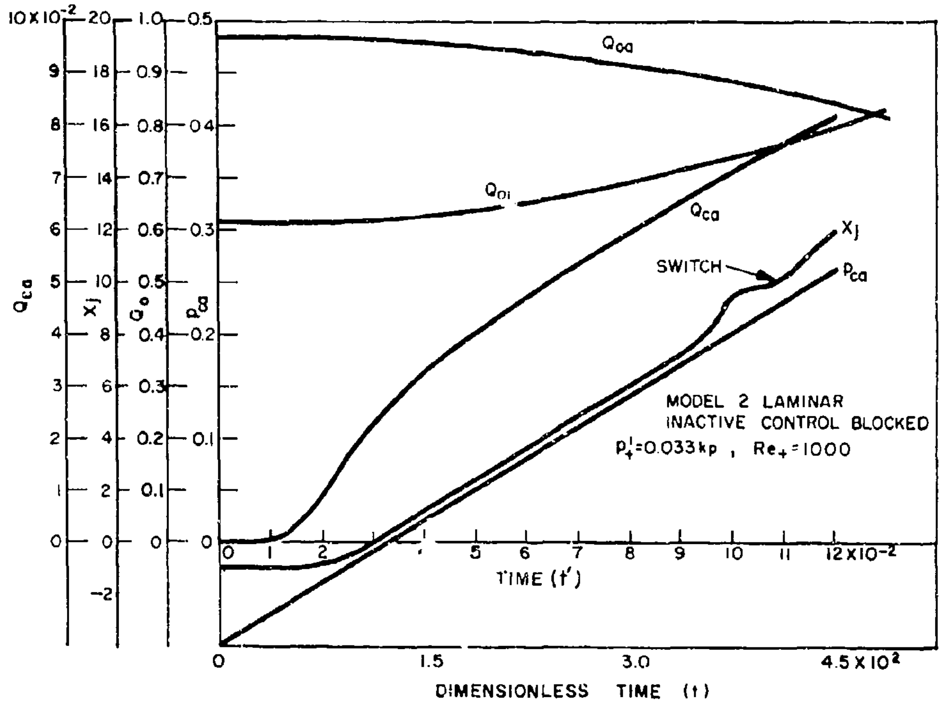

Figure 27. Laminar switching times, Model 2.

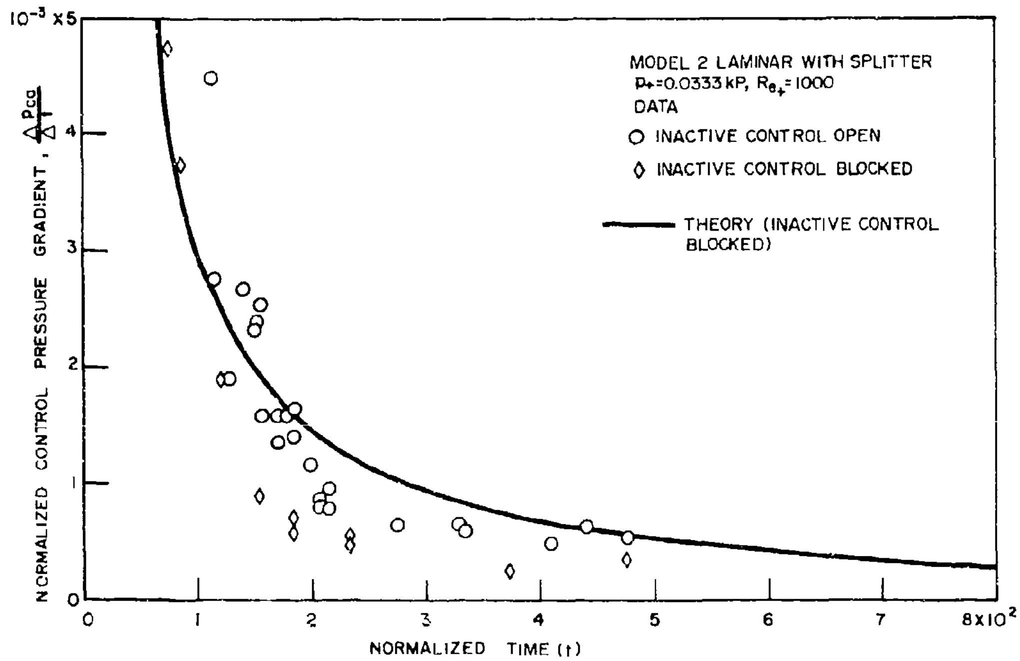

Figure 28. Analytical laminar output variables during switching, Model 2.

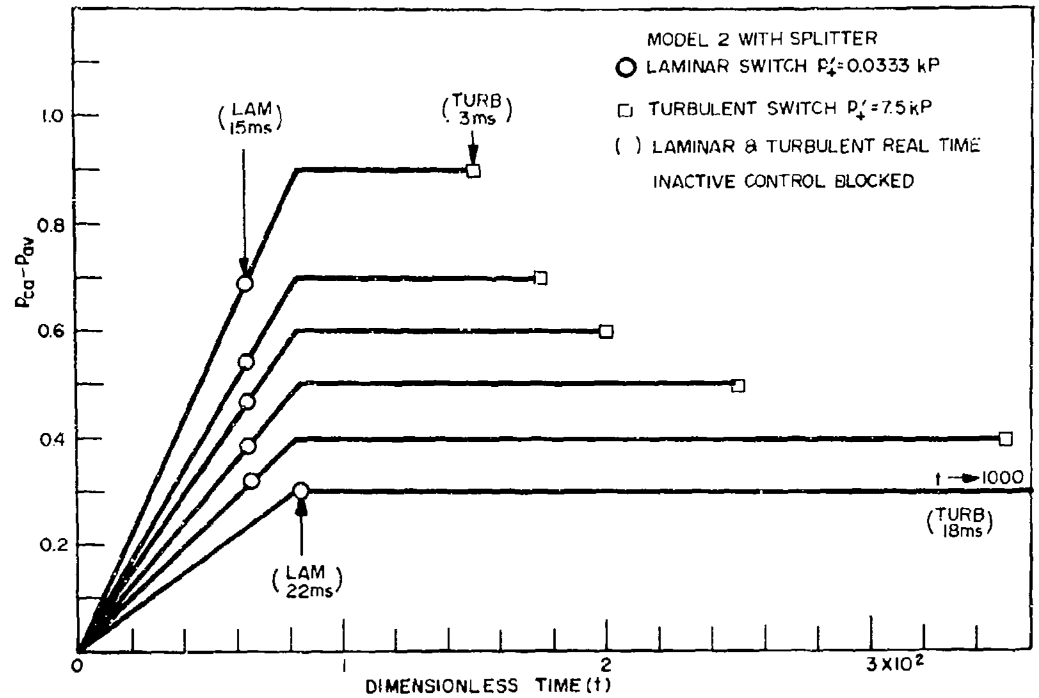

Figure 29. Comparison of laminar and turbulent switch times.

history of all the problem variables can be determined. A flueric wall-attachment amplifier of the design shown in figure 30 was tested. Important features of this particular amplifier are: (1) the control resistances do not depend directly on the spacing between the jet and the wall when the corner is cut away because the smallest area through which the control flow passes into the bubble is the control nozzle; (2) the measured output pressure is the dynamic pressure issuing into the vented region; (3) the offset of zero and the wall angle is 0.21 rad; and (4) loading the outputs has no effect on the flow regime in the amplifier interaction region due to the decoupling action of the large vent region.

Figure 31 and 32 show oscilloscope traces of the amplifier response, and figure 33 shows the comparison between the predicted and the measured response. Note that the predicted response does not exhibit the overshoot of the data. This overshoot or "ringing" seems to be attributable to the Helmholtz response of the output passage coupled to the transducer cavity; otherwise, the agreement is good. It is important to note that the divergence of figure 19 does not occur when the jet attaches to the opposite side. This shows that the results are truly indicative of the actual mechanisms occurring in an amplifier.

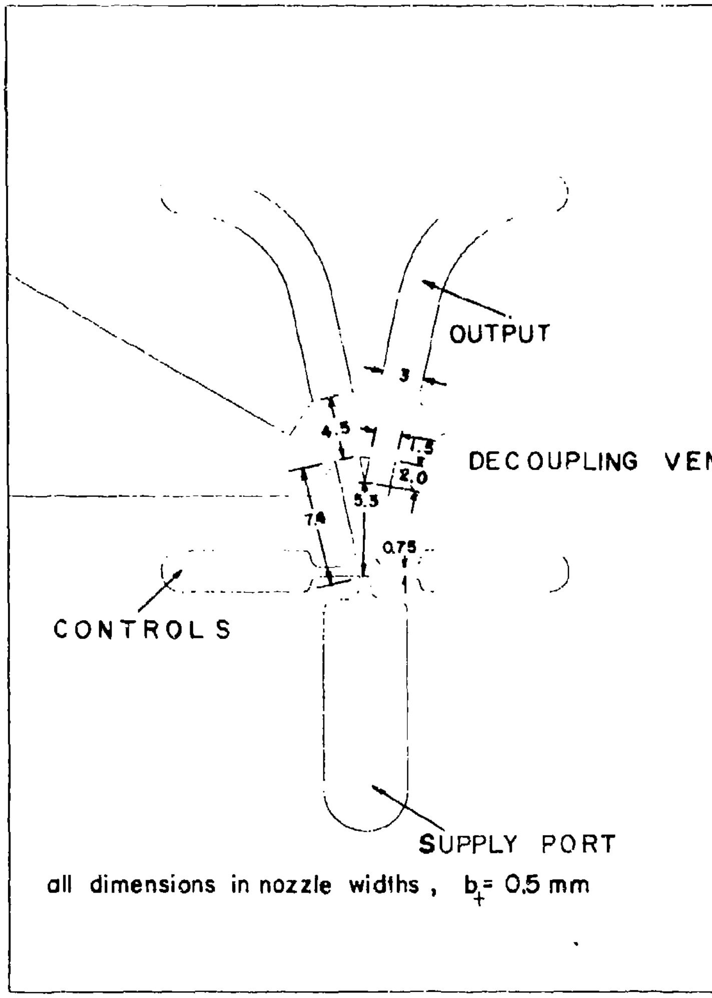

Figure 30. Flueric bistable wall attachment amplifier

5. REMARKS AND CONCLUSIONS

We have shown that the two-dimensional turbulent and laminar jet analytical models agree with experimental results obtained from several different flueric, bistable amplifier geometries. The theory allows the calculation of the steady-state jet attachment point location, jet switching times with and without a splitter, and amplifier output response.

Application of the present theory for low attachment-wall offsets can be justified because of the agreement with Johnston's data[14] and the results presented in section 4.6. Note that the jet centerline intersected the opposite wall during the analytical calculations for both cases. As noted previously, the jet touching and flowing along the opposite wall is not considered as a separate mode of switching. This

Figure 31. Oscilloscope trace of control and active output pressure during switching.

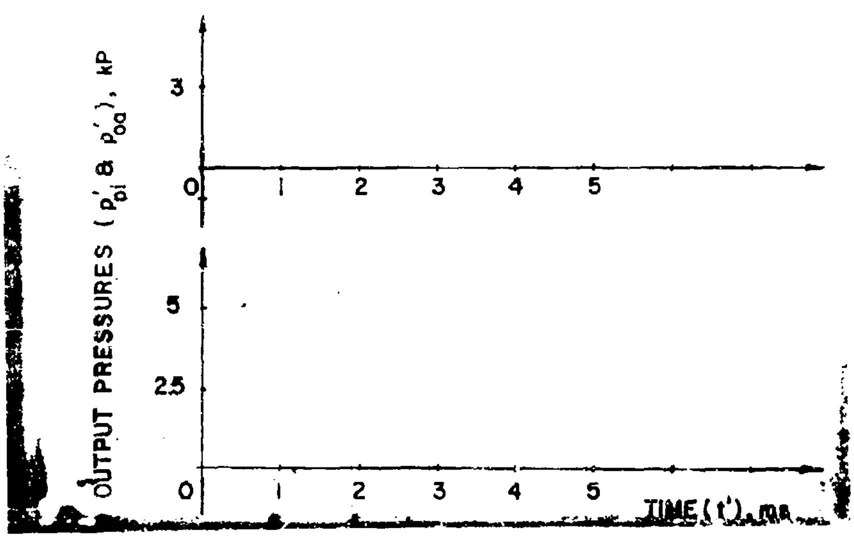

Figure 32. Oscilloscope trace of output pressures during switching.

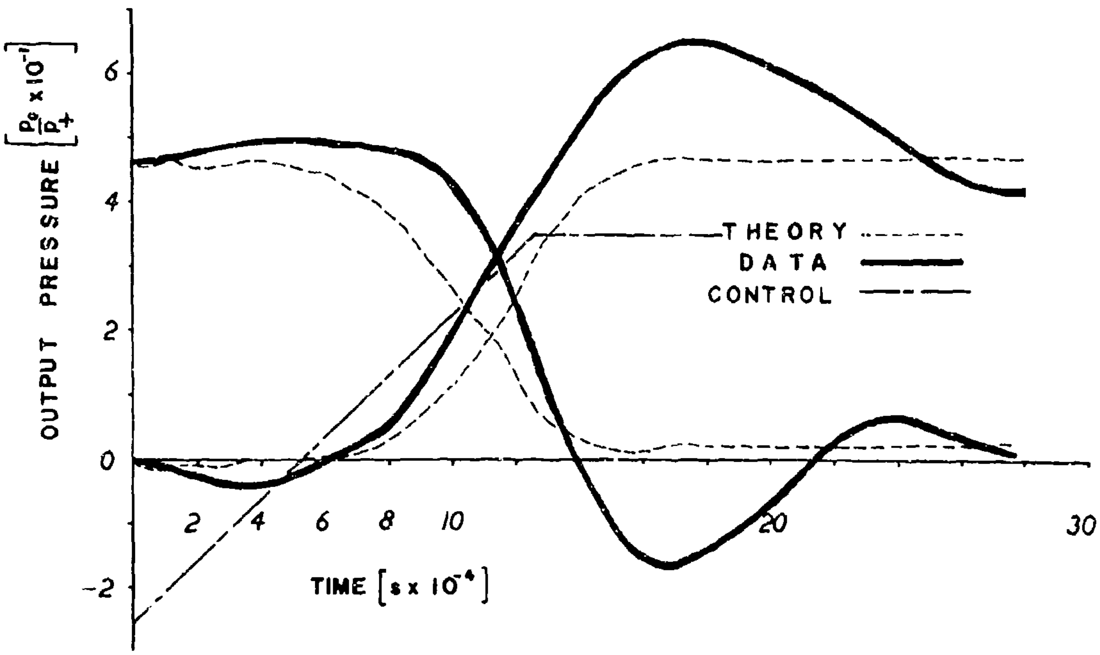

Figure 33. Comparison of theoretical switching response with experimentally observed data.

implies that attachment to the opposite wall and at the same time to the original attachment wall does not result in a self-sustaining process ending with a switch. Muller's data[15](fig. 10, 11, and 14 of reference 15) indicate that the jet will return to its original position after flowing along the opposite wall unless a minimum control pulse duration is exceeded. Keto[16] concluded from his experimental evidence that the attachment bubble must be broken, or vented to some other port before a switch can be considered self-sustaining. Since the opposite wall deforms and even restrains the size of the bubble rather than bursts it, the present model's assumption, where the bubble shape is altered when the jet flows along the opposite wall, is justified.

The agreement obtained for the laminar jet switching is particularly satisfying as the present trend in fluidics is for low power consumption devices. The laminar model is not concerned with whether or not the jet is actually laminar, but rather whether or not the analytical laminar jet velocity profile expression is suitable for use in predicting the jet response at the lower Reynolds number. The laminar numerical results from which the switching characteristics of section 4.4 are obtained indicate that a significant portion of the flow is directed toward the opposite output line. In the usual bistable device, flow out of the inactive output may be undesirable; however, if the amplifier is operated differentially, it may be of little consequence. The good laminar results indicate, however, that laminar devices should be investigated and that the present analytical model can be used to describe them.

[16]Keto, J.R., "Transient Behavior of Bistable Fluid Elements," Proc. 2nd Fluid Amplification Symposium, HDL, Vol. III, May 1964.

The jet-spread parameter σ for the turbulent model is the only parameter in the analysis that cannot be specified arbitrarily. The value of $\sigma = 10$ used in the analysis is based on the experimental results of others and is assumed constant for all wall-attachment amplifiers (at least for the range of aspect ratios of one to 3.3 of the models for which comparisons have been made). The general agreement of the theory indicates that the use of one constant value for σ is justified. Changing σ as much as 20 percent in the calculations does little in changing the switching time.

From the designer's viewpoint, the model is versatile because the switching time as well as the total response time is available from the computer solution. Analytical results for all other variables such as flows and pressures are also available. From computer input and output data, quantities such as pressure and flow recovery, pressure and flow gain, fan out, and steady-state characteristic curves are obtainable if desired, and the present results show that this is feasible.

Future refinements to the model should include consideration of blunt and cusped splitter fluid amplifiers. The potential of the present model may also be increased by including asymmetrical geometries, curved attachment walls and temperature effects through known relationships between density, viscosity and temperature.

LIST OF SYMBOLS

A area per unit depth

AR aspect ratio = depth/nozzle width

b nozzle width

B amplifier half-width at the downstream edge of the control

c_d discharge coefficient

C laminar jet coefficient

d distance along attachment wall

D attachment wall offset distance

F force

h unit depth

k jet profile coefficients

K resistive parameter

L inductive parameter

m vortex velocity function coefficient

n coordinate perpendicular to jet centerline

p pressure

Q volumetric flow rate per unit depth

r radial distance associated with bubble vortex

R jet radius of curvature

R_e Reynolds number = $\frac{b'u'}{\nu'} = \frac{Q'_+}{\nu}$

s coordinate distance measured along jet centerline from supply exit plane

t time

T attachment parameter

u velocity

V volume per unit depth

W line area per unit depth

x coordinate distance along axis of unit

y coordinate distance normal to x

Δy_c displacement of jet centerline from geometric axis measured at downstream edge of control

z distance along a streamtube

α attachment wall angle

β jet deflection angle

ζ angle associated with vent restriction

η similarity parameter-turbulent

θ jet attachment angle

λ subsidiary attachment variable

ν kinematic viscosity

ξ similarity parameter-laminar

ρ density

σ turbulent jet spread parameter

ψ angular coordinate

ω angular velocity of bubble vortex

subscripts

a active side (side to which jet is initially attached)

ap attachment point

av average value

b attachment bubble

c control

ca active control (control on initial attachment side)

ci inactive control (control opposite initial attachment side)

d dynamic (except for the discharge coefficient c_d)

e entrainment

em associated with vortex velocity

i inactive side (side opposite initial attachment side)

j point where jet centerline intersects unit axis

o output

oa active output

oi inactive output

q actual flow

r returned

s supply exit

sp leading edge of splitter

t total conditions

v vent

va active-side vent

vi inactive-side vent

vo virtual origin of jet

w point where jet centerline intersects attachment wall

+ invariant supply, source, or reference condition

superscript

Prime denotes dimensional form

APPENDIX A

```
*  DSL/90 LISTING FOR MODEL 1, MODEL 2 (LAMINAR AND TURBULENT),
*  AND MODEL 3.
*
*
$JOB           179302-T,15,50000,DRZEWI RETURN TO BLDG 92
$*    DSL/90   MOUNT TAPE S-72 (DSL90) ON B5, SCRATCH ON A5
$EXECUTE       USER
$DSL90
$IEDIT         SYSCK2,SCHF4
$IBLDR MAIN
$IEDIT
*
* THIS PROGRAM SIMULATES THE EQUATIONS GOVERNING THE TRANSIENT RESPONSE
*  OF A BISTABLE AMPLIFIER WITH OUTPUT LINES
*
*INITIAL CONDITIONS ARE ARBITRARY. FOR THIS PROGRAM THETAO=0.6
*                                                   V0=6.0
*                                                   QS0=1.0
*                                                   QC10=QC20=QV10=0.0
*                                                   QV2=.2,QO1=2.0
*                                                   QO2=.5,PLEVELO=.2
*THESE CONDITIONS WILL GENERATE THE ACTUAL INITIAL CONDITIONS FOR THE
*PROBLEM BY TIME=FINTIM/2.0
*   FINTIM IS TOTAL RUN TIME IN SECONDS. FIRST HALF OF FINTIM IS USED
*   TO CALCULATE THE INITIAL CONDITIONS FOR THE PROBLEM GIVEN, THE
*   SECOND HALF IS USED TO COMPUTE THE TRANSIENT RESPONSE TO THE GIVEN
*    INPUTS
*
* THERE ARE TEN DIRECT OUTPUTS
*  TIME(SECONDS),DIMENSIONLESS TIME, REATTACHMENT POINT,CENTERLINE OF
*  JET LOCATION,ACTIVE CONTROL FLOW,INACTIVE CONTROL FLOW,ACTIVE OUTPUT
*  LINE FLOW,INACTIVE OUTPUT LINE FLOW,ACTIVE OUTPUT DYNAMIC PRESSURE,
*  INACTIVE OUTPUT DYNAMIC PRESSURE
*
*BASIC DIMENSIONAL PARAMETERS
*  TIME=SECONDS
*  TRISE= RISE TIME OF INPUT PRESSURE SIGNAL,SEC
*  TAUTR=THE TRANSPORT TIME FOR ONE NOZZLE WIDTH B0 AT PRESSURE P0, SEC
* FLUID CHARACTERISTICS
*  RHO=DENSITY, KILOGRAM/CUBIC METER
*  NU=KINEMATIC VISCOSITY, METER SQRD/SEC
* AMPLIFIER
* SUPPLY
*  B0=SUPPLY NOZZLE WIDTH, METERS
*  B02=B0 SQRD, METERS SQRD
*  P0=SUPPLY PRESSURE, KILOPASCAL
*  UPLUS=SUPPLY REFERENCE VELOCITY, M/SEC
*       CCEF 44.72=CONVERSION FACTOR OF SQRT(2.*1000)
*  CONV=REF VOL FLOW PER UNIT DEPTH FOR 0. EXIT PRES, METER SQRD/SEC
* INPUTS
*  T1,T2=TIME CONTROL INPUTS ARE APPLIED, SECONDS
*  Z1,Z2=FORCING FUNCTION OF UNITY AMPL APPLIED AT TIME T1,T2
*
*BASIC NONDIMENSIONAL PARAMETERS
* TIME
*  TNOND=TIME NONDIMENSIONALIZED WITH TAUTR
```

```
* JET CHARACTERISTICS
*  RE=REYNOLDS NUMBER BASED ON REFERENCE VOLUME FLOW
*  REC1,REC2= CONTROL REYNOLDS NUMBERS
*  SIGMA=TURBULENT JET SPREAD PARAMETER
*  C1,C2=LAMINAR JET COEFFICIENTS
*  SO=UPSTREAM DIST TO APPARENT JET SOURCE  LAMINAR JET
* AMPLIFIER GEOMETRY
*  CLOSE1,CLOSE2=0. FOR A CONTROL THAT IS OPEN OR HAS A SIGNAL
*  CLOSE1,CLOSE2=1. FOR A CONTROL THAT IS CLOSED AND CAN HAVE NO SIGNAL
*  PRE1,PRE2=0. FOR OPEN CONTROLS DURING INCON CALC
*  PRE1,PRE2=1. FOR CLOSED CONTROL DURING INCON CALC
*  POST1,POST2=0. FOR OPEN CONTROL DURING TIME RESPONSE CALC
*  POST1,POST2=1. FOR CLOSED CONTROL DURING TIME RESPONSE CALC
*  ALPH=ATTACHMENT WALL ANGLE (RADIANS)
*  D=SETBACK
*  BC=CONTROL WIDTH
*  BC2=CONTROL WIDTH SQUARED
*  XV1=DISTANCE ALONG ATTACHMENT WALL TO VENT
*  LGTHS=LENGTH OF SUPPLY CHAMBER
*  AREAS=CROSS SECT. AREA/UNIT DEPTH OF SUPPLY CHAMBER
*  LGTHC=LENGTH OF CONTROL CHANNEL
*  AREAC=CROSS SECT. AREA/UNIT DEPTH OF CONTROL CHANNEL
*  LGTHV=LENGTH OF VENT CHANNEL
*  AREAV=CROSS SECT. AREA/UNIT DEPTH OF VENT CHANNEL
*  LGTHR= LENGTH OF OUTPUT LINES
*  AREAR= CROSS-SECTIONAL AREA OF OUTPUT LINE
*
*PROBLEM VARIABLES
* VELOCITY
*  UE=BUBBLE VORTEX DRIVING VELOCITY
*  UE2=SQUARE OF BUBBLE VORTEX DRIVING VELOCITY
*  UEM=MAX VORTEX DRIVING VEL BASED ON ENTRAINMENT STREAMLINE
*  M1,M2=MATCHING COIF FOR THE VORTEX VELOCITY FUNCTION
* FLOW
*  V=CONTINUITY EQ INTEGRAL FOR THE BUBBLE VOLUME
*  QS=SUPPLY FLOW
*  QS2=SUPPLY FLOW SQUARED
*  QC1,QC2=CONTROL FLOW
*  QV1=VENT FLOW
*  QV2= FLOW THROUGH THE OPPOSITE SIDE VENT
*  QR1=RETURNED FLOW
*  QE1=ENTRAINED FLOW
*  QO1QO2= FLOWS THROUGH THE OUTPUT LINES
*  QS0,V0,QC10,QC20,QV10,QV20,QO10,QO20 INITIAL CONDITIONS FOR INTEGRALS
*  QO1AVL= SUM OF ALL FLOWS ENTERING AMPLIFIER EXCEPT BY THE ACTIVE
*         OUTPUT
* PRESSURE
*  PC1,PC2=CONTROL PRESSURE INPUT FORCING FUNCTIONS
*  P1,P2=PERCENT OF SUPPLY PRESSURE TO CONTROL
*  P1BIAS,P2BIAS=CONTROL BIAS LEVEL
*  PB1=ATTACHED SIDE BUBBLE PRESSURE
*  PB2=UNATTACHED SIDE PRESSURE
*  DELPB=PRESSURE DIFFERENCE ACROSS JET=PB2-PB1
*  PAV=AVERAGE PRESSURE AT EXIT OF SUPPLY AND CONTROLS
*  PSY= SUPPLY NOZZLE EXIT PRESSURE
*  P1B,P2B= CONTROL EXIT PRESSURES
*  PV1=AMBIENT PRESSURE AT VENT
*  PV2= PRESSURE AT OUTSIDE OF THE OPPOSITE SIDE VENT
*  PO1,PO2= EXIT PRESSURES OF THE OUTPUT LINES
*  PRISE= TRANSIENT VALUES OF INPUT PRESSURE DURING THE RISE TIME
```

```
*  DPDT= GRADIENT OF INPUT PRESSURE SIGNAL
*  PD1,PD2= DYNAMIC PRESSURES IMPINGING ON THE OUTPUT LINES
*  POUT1,POUT2= TOTAL PRESSURES IMPINGING ON THE OUTPUT LINES
*  PDOUT1,PDOUT2= DYNAMIC PRESSURES AT THE END OF THE OUTPUT LINES
*  PLEVEL= PRESSURE LEVEL IN AMPLIFIER MEASURED AT EDGE OF THE BUBBLE
*          VORTEX
*  DP= INCREMENTAL PRESSURE CHANGE DUE TO MISMATCH BETWEEN AVAILABLE
*      FLOW AND DEMAND FLOW
* LINE CHARACTERISTICS
*  RC1,RC2=CONTROL RESISTANCE
*  RCMIN1,RCMIN2= MINIMUM CONTROL RESISTANCES
*  RCMAX=MAX CONTROL RESISTANCE BASED ON ENTRAINED WIDTH OF 8 DEG JET
*        SPREAD AT CONTROL EDGE
*  RC1D,RC2D=DIST BETWEEN JET EDGE AND WALL (KC+DYC),(KC-DYC) AT CONTROL
*  D1,D2= CONTROL DISCHARGE COEFFICIENTS
*  D12,D22= CONTROL DISCHARGE COEFFICIENTS SQUARED
*  CDMIN,CDMAX= MINIMUM AND MAXIMUM DISCHARGE COEFFICIENTS OVER RANGE
*               OF OPERATION OF THE CONTROLS
*  CS= SUPPLY NOZZLE DISCHARGE COEFFICIENT
*  RV1=VENT RESISTANCE
*  RV2= RESISTANCE OF OPPOSITE SIDE VENT
*  RO1,RO2= RESISTANCES OF THE OUTPUT LINES
*  LS=SUPPLY INDUCTANCE
*  LC=CONTROL INDUCTANCE
*  LV=VENT INDUCTANCE
*  LV2= INDUCTANCE OF OPPOSITE SIDE VENT
*  LO= INDUCTANCE OF OUTPUT LINE
* MOMENTUM
*  FC1,FC2= FORCES ACTING TO DEFLECT THE JET AT THE CONTROLS
*  FSY= JET MOMENTUM FLUX EQN AT THE INTERACTION REGION
*  BETA=DEFLECTION ANGLE DUE TO SUPPLY AND CONTROL JET INTERACTION
*  ZET= ANGLE WHICH DETERMINES POINT AT WHICH MOMENTUM IS FIRST PEELED
*       OFF
*  XSI= ANGLE DETERMINING AMOUNT OF PEELED OFF MOMENTUM
*  YS= REMAINING WIDTH ON OFF SIDE OF JET AFTER PEELING OFF
*  TS= MOMENTUM REMAINING ON OFF SIDE OF JET TO ARRIVE AT REATTACHMENT
*      POINT
*  T=NO LOSS MOMENTUM EQ AT ATTACHMENT POINT
*  B= ARGUEMENT OF ROOT OF REATTACHMENT POINT EQN
* GEOMETRY
*  R=RADIUS OF CURVATURE OF JET CENTER LINE (CL)
*  VCL=REATTACHMENT BUBBLE VOL ENCLOSED BY JET CL
*  XCL=DISTANCE ALONG WALL TO CENTER LINE ATTACHMENT POINT
*  XAP=DIST ALONG WALL TO RETURNED FLOW ATTACHMENT POINT
*  LSP=DIST TO INTERSECTING OF JET CL AND AMPL CL
*  SPL=SPLITTER DISTANCE
*  CO1==DIFFERENCE BETWEEN VENT AND ATTACHMENT POINT DISTANCE
*  THETA=INTERSECTION ANGLE OF JET CENTER LINE AT ATTACHMENT
*  S1=ARC LENGTH OF JET FROM EXIT TO ATTACHMENT
*  SF=HALF S1=LOCATING ARC LENGTH FOR VORTEX CENTER LINE IN BUBBLE
*  SEM=ARC LENGTH ASSOCIATED WITH THE VELOCITY UEM
*  SV=ARC LENGTH OF JET CL TO RADIAL LINE THRU VENT EDGE
*  ZETA=ANGLE FOR CALC ARC LENGTH SV
*  Y1=NORMAL DIST FR JET CL TO RETURNED FLOW STREAMLINE AT ATTACHMENT
*  YV=NORMAL DIST FR JET CL TO RETURNED FLOW STREAMLINE
*  KC=DIST FROM EDGE OF CONTROL TO EDGE OF NO-SPREAD, UNDEFLECTED JET
*  DYC=LATERAL DISPLACEMENT OF JET MEASURED AT CONTROL EDGE
*  DV=EFFECTIVE RESTRICTION FOR VENT FLOW
*  X1,X2,=CL COORD WHERE JET RADIUS INTERSECTS OPPOSITE WALL
*  XI1=ANGLE SUBTENDED BY SUPPLY EXIT POINT AND X1
```

```
*  XI2=ANGLE SUBTENDED BY X1 AND X2
*  SWO=ARC SUBTENDED BY XI2
*  LEW=DIST ALONG OPPOSITE WALL SUBTENDED BY XI2
*  WL=RATIO OF LEW/SWO
*
* COMPUTATIONAL VARIABLES
*  L=1. LAMINAR CASE
*  L=0. TURBULENT CASE
*  E=0. IF ATTACHMENT POINT HAS NOT REACHED VENT EDGE. IF IT HAS, E=1.
*  RT=1. TERMINATES SIMULATION
*  TTT=INITIALIZING CONSTANT
*  TTTT= INITIALIZING FACTOR FORINPUT RAMP GRADIENT CALCS
*  IT= ITERATIVE COUNTER IN PRESSURE LEVEL CALCS
*  TINCON=TIME THE INCONS ARE CALC
*  SA,CA,CA2,TA,A1,A2,A3,A4,C3,C4,C7=CALCULATED CONSTANTS
*  GAM,SG,CG,ST,CT,SB,CB,CB2=SUBSIDIARY CALC. OF VARIABLE TRIG FUNCTIONS
*  B2,BW,BW2,CW,SUM1,CBR,CBL,SV1=SUBSIDIARY ALGEBRAIC AND TRIG CALC.
*  SAD,GAD=ARGUMENT AND SUBSIDIARY CALC FOR THETA IMPLICIT LOOP
*  QV1I,ARGQV1,QV1DOT= COMBINATION FOR CALCULATING VENT FLOW QV1
*  PLUS= SIGN OF DIFFERENCE BETWEEN AVAILABLE FLOW AND DEMAND FLOW
*  THETAO=INITIAL QUESS FOR THETA IMPLICIT LOOP
*  PLEVELO= INITAL GUESS AT THE PRESSURE LEVEL IN THE AMPLIFIER
*  ARGN=SQRT FUNCTION ARGUMENTS
*  ROOTN=SQRT OF ARGN
*
*
01401 FORMAT(/, 9H INCON V=,F8.4,7H THETA=,F8.4,3H R=,F8.4,5H QC1=,F8.4,
0    15H QC2=,F8.4,5H QV1=,F8.4,4H QS=,F8.4,/)
NOSORT
      IF(TIME.GT.0.) GO TO 10
      UPLUS=44.72*SQRT(PO/RHO)
      CONV=BO*UPLUS
      RE=CONV/NU
      TAUTR=BO/UPLUS
      PB2=1.-QSO**2*(1.-1./(2.*RO))
      PAV=1.-QSO**2*(1.+1./(2.*RO))
      PSY=.5*(PAV+PB2)
      BO2=BO*BO
      BC2=BC*BC
      SA=SIN(ALPH)
      CA=COS(ALPH)
      CA2=CA*CA
      TA=TAN(ALPH)
      A1=3./SIGMA
      A2=(D+.5)*CA
      A3=(D+.5)*SA
      A4=(D+.5)*TA
      C3=C1/C2
      C4=(C2/(2.*C1))**3
      C7=.5*C2/(2.*C1)**2
      LC=2.*LGTHC/AREAC
      LS=2.*LGTHS/AREAS
      KC=D+BC*TA
      KCMAX=1./(.1414*BC)**2
      AREAR=A2+SPL*SA
      LO=2.*LGTHR/AREAR
      LV2=2.*LGTHV/AREAV
      RO1=1./AREAR**2
      RO2=1./AREAR**2
      RV2=1./AREAV**2
```

```
      RV11=1./AREAV**2
      IF(L.GT.0.) GO TO 9
      UEM=SQRT(1./3.)
      SEM=2./A1
    9 CONTINUE
*
*PROGRAM INITIAL CONDITIONS
*
      T1=10.0E5
      T2=10.0E5
      TTT=0.0
      TTTT=0.
      TINCON=0.0
      CLOSE1=PRE1
      CLOSE2=PRE2
      WL=0.
      XI2=0.
      RT=0.
      PLEVEL=PLEVLO
      IT=0.0
*
   10 CONTINUE

*     START CALC OF DISCHARGE COEFF AND MIN RESISTANCES
*
      REC1=ABS(QC1*RE)
      REC2=ABS(QC2*RE)
      IF(REC1.LT.2500.) GO TO 1
      D1=-(CDMAX-CDMIN)*REC1/1.E4+1.25*CDMAX-.25*CDMIN
      GO TO 2
    1 IF(REC1.GT.1000.) GO TO 5
    5 D1=CDMAX
    2 IF(REC2.LT.2500.) GO TO 3
      D2=-(CDMAX-CDMIN)*REC2/1.E4+1.25*CDMAX-.25*CDMIN
      GO TO 4
    3 IF(REC2.GT.1000.) GO TO 6
      GO TO 4
    6 D2=CDMAX
    4 CONTINUE
      D12=D1*D1
      D22=D2*D2
      RCMIN1=1./(BC2*D12)
      RCMIN2=1./(BC2*D22)
*
*       END CALC OF DISCHARGE COEFF AND MIN RESISTANCES
*
*THE FOLLOWING GENERATES THE INITIAL CONDITION PRINTOUT AND STARTS
*  THE TIME DEPENDENT PROBLEM
*
      IF(TIME.LT.FINTIM/2.) GO TO 15
      IF(TTT.GT.0.) GO TO 15
      TTT=1.0
      T1=TIME
      T2=TIME
      TINCON=TIME
      CLOSE1=POST1
      CLOSE2=POST2
      WRITE(6,1401) V,THETA,R,QC1,QC2,QV1,QS
   15 CONTINUE
*
```

```
*END OF TIME LOOP
*
*
*      START CALC OF PRESSURE LEVEL
*
       IF(TIME.LE.IT) GO TO 99
       Q01AVL=QS+QC1+QC2+QV1+QV1A+QV2+Q02
       PLUS=SIGN(1.,Q01AVL-Q01)
       DP=R01*PLUS*(Q01-Q01AVL)**2
       PLEVEL=PLEVEL+DP
       IT=TIME
 99    CONTINUE
*
*        END CALC OF PRESSURE LEVEL
*
       TNOND=(TIME-TINCON)/TAUTR
       Z2=STEP(T2)
*
*      START CALC FOR JET DEFLECTION
*
       QS2=QS*QS
       IF(QC2.GE.0.0) FACTOR=1.0
       IF(QC2.LT.0.0) FACTOR=0.0
       FC1=(PAV+2.*(QC1/BC)**2)*BC
       FC2=(PB2+2.*(QC2*FACTOR/BC)**2)*BC
       FSY=PSY+2.*QS2
       BETA=ATAN((FC1-FC2)/FSY)
*
*        END CALC FOR JET DEFLECTION
*
       GAM=(ALPH+BETA)
       SG=SIN(GAM)
       CG=COS(GAM)
       VCL=V+.5*R*R*(XI2-SIN(XI2))
       B2=A2**2/(2.*VCL+A2*A4)
*
*      START IMPLICIT ROUTINE FOR ATTACHMENT ANGLE THETA
*
       THETA=IMPL(THETA0,1.E-3,GAD)
       ST=SIN(THETA)
       CT=COS(THETA)
       ROOT1=(B2*(SG+.5*ST)-CG)**2-CG*CG+B2*(GAM+THETA+.5*SIN(2.*GAM))
   803 SAD=ARCOS(-B2*(SG+.5*ST)+CG-SQRT(ABS(ROOT1)))
       GAD=ABS(SAD)
*
*        END IMPLICIT ROUTINE FOR ATTACHMENT ANGLE THETA
*
*      START CALC OF GEOMETRIC VARIABLES
*
       R=A2/(CG-CT)
       S1=R*(GAM+THETA)
       SB=R*SIN(BETA)
       CB=R*COS(BETA)
       CB2=CB*CB
       IF(BETA) 29,29,20
    20 BW=CA2*(A4+TA*CB-SB)
       BW2=BW*BW
       CW=A2*A2+2.*A2*CA*CB
*
*STATEMENTS 25-29 CALC IF JET CL INTERSECTS OPPOSITE WALL
```

```
*
   25 IF(BETA.LT.ALPH) GO TO 29
      ARG5=BW2-CW
      IF(ARG5.LT.0.) GO TO 29
      ROOT5=SQRT(ARG5)
      X1=-BW-ROOT5
      X2=-BW+ROOT5
      IF(X1.LT.0..OR.X2.LT.0.) GO TO 29
      XI1=BETA-ARSIN((SB-X1)/R)
      XI2=BETA-XI1+ARSIN((X2-SB)/R)
      SWO=R*XI2
      LEW=2.*R*SIN(XI2/2.)
      WL=LEW/SWO
   29 CONTINUE
*
*        END OPPOSITE SIDE INTERSECTION EQNS
*
*     START CALC FOR MOMENTUM PEELED OFF BY SPLITTER
*
      ZET=ATAN(CB/(SPL-SB))
      IF(ZET.GT.(PI/2.-THETA-ALPH)) GO TO 31
      TS=1.0
      GO TO 28
   31 CONTINUE
      SS=R*(BETA-ZET+PI/2.)
      XSI=SQRT(CB**2+(SPL-SB)**2)
      YS=XSI-R
*
*        END CALC FOR MOMENTUM PEELED OFF BY SPLITTER
*
*     START CALC OF MOMENTUM AT ATTACHMENT POINT
*
      IF(L.GT.0.) GO TO 27
      SO=SIGMA/3.
      TS=TANH((YS*SIGMA)/(SS+SO))
      GO TO 28
   27 SO=C4*RE*QS
      TS=TANH(YS*C2*(QS*RE/(SS+SO))**(2./3.))
   28 CONTINUE
      B=1.5*(-TS+(TS**3/3.)+2./3.+(2./3.+TS-(TS**3/3.))*COS(THETA))
      T=2.*COS((2.*PI-ARCOS(-B/2.))/3.)
*
*        END CALC OF MOMENTUM AT ATTACHMENT POINT
*
*     START ENTRAINED FLOW AND RETURNED FLOW CALCS
*
      IF(L) 30,30,40
   30 ARG6=A1*S1+1.
  911 ROOT6=SQRT(ARG6)
      QR1=.5*QS*ROOT6*(1.-T)
      QE1=.5*QS*(ROOT6-1.)
      GO TO 49
   40 SUM1=S1+SO
      SUM1=S1+SO
      CBR=(QS2/RE)**(1./3.)
      QR1=C3*CBR*SUM1**(1./3.)*(1.-T)
      QE1=C3*CBR*SUM1**(1./3.)-.5*QS
      SEM=SO*(SQRT(27.)-1.)
      UEM=C1*(2.*C3-1./3.)/SQRT(3.)*QS
   49 CONTINUE
```

```
*
*        END ENTRAINED FLOW AND RETURNED FLOW CALCS
*
      ARG8=CB2-BC2+2.*BC*SB
  917 ROOT8=SQRT(ARG8)
      DYC=-CB+ROOT8
*
*BEGIN CALC FOR CONTROL RESISTANCE
*
      RC1D=1./((KC+DYC)**2+1.E-5)
      RC2D=1./((KC-DYC)**2+1.E-5)
      IF(RC1D.GE.RCMIN.AND.RC1D.LE.RCMAX) RC1=RC1D
      IF(RC1D.GT.RCMAX) RC1=RCMAX
      IF(RC1D.LT.RCMIN1) RC1=RCMIN1
      IF(RC2D.GE.RCMIN.AND.RC2D.LE.RCMAX) RC2=RC2D
      IF(RC2D.GT.RCMAX) RC2=RCMAX
      IF(RC2D.LT.RCMIN2) RC2=RCMIN2
      IF(RC1.EQ.RC1D) D1=1.
      IF(RC2.EQ.RC2D) D2=1.
*
*END CALC FOR CONTROL RESISTANCE
*
*BEGIN CALC FOR VENT RESISTANCE
*
      ZETA=ATAN((XV1*CA-SB)/(CB-D-.5-XV1*SA))
      SV=R*(BETA+ZETA)
 1701 IF(L.GT.0.) GO TO 1704
      Y1=(A1*S1+1.)/6.*ALOG((1.+T)/(1.-T))
      YV=Y1*(A1*SV+1.)/(A1*S1+1.)
      GO TO 1705
 1704 Y1=C7*(1.*(S1/S0+1.))**(2./3.)*ALOG((1.+T)/(1.-T))
      YV=Y1*((SV+S0)/(S1+S0))**(2./3.)
 1705 CONTINUE
      XCL=R*(SG+ST)-A3
      XAP=XCL-Y1/SIN(THETA)
      C01=XAP-XV1
      E=COMPAR(XAP,XV1)
      IF(E.GT.0.) GO TO 400
      DV=0.
      GO TO 401
  400 DV=R-YV-((XV1*CA-SB)/SIN(ZETA))
  401 CONTINUE
      IF(E.GT.0.) GO TO 500
      RV1=0.
      GO TO 502
  500 IF(C01.LT.AREAV) GO TO 501
      RV1=1./AREAV**2
      GO TO 502
  501 RV1 =1./(DV**2+1.E-5)
  502 CONTINUE
*
*END CALC FOR VENT RESISTANCE
*
*BEGIN CALC FOR BUBBLE VORTEX VELOCITY
*
      SE=.5*S1
      IF(SE.LE.SEM) GO TO 602
      IF(L.GT.0.) GO TO 700
*
*VORTEX DRIVING VEL BASED ON ENTRAINMENT  TURBULENT
```

```
*
      SE1=1./(A1*SE+1.)
      UE2=2.25*SE1*(1.-SE1)*(1.-SE1)*QS2
      GO TO 701
*
*VORTEX DRIVING VEL BASED ON CUBIC EQ  LAMINAR AND TURBULENT
*
  602 M1=2.*(QS-UEM)/(SEM**3)
      M2=-1.5*M1*SEM
      UE=M1*SE**3+M2*SE**2+QS
      UE2=UE*UE
      GO TO 701
*
*VORTEX DRIVING VEL BASED ON ENTRAINMENT  LAMINAR
*
  700 CBL=(RE*QS/(SE+SO))**(1./3.)
      UE=C1*QS*CBL*(1.-(C2/(2.*C1))**2*(CBL**2))
      UE2=UE*UE
  701 CONTINUE
*
*END CALC FOR BUBBLE VORTEX VELOCITY
*
      PB1=-.5*UE2+PLEVEL
      DELPB=2.*QS2/R
      PB2=PB1+DELPB
      PAV=.5*(PB1+PB2)
      PSY=.5*(PAV+PB2)
*
*     START CALC OF INPUT RAMP GRADIENT
*
      IF(TIME.LT.FINTIM/2.) GO TO 16
      IF(TTTT.GT.0.) GO TO 16
      DPDT=(P1-PAV)/(TRISE/TAUTR)
      PB10=PAV
      TTTT=1.
   16 CONTINUE
*
*       END CALC OF INPUT RAMP GRADIENT
*
*  CONTROL RAMP
*
      IF(TIME.GT.TRISE+FINTIM/2.) GO TO 7
      PRISE=(P1-PB10)*(TIME-FINTIM/2.)/TRISE+PB10
      GO TO 8
 7    PRISE=P1
    8 CONTINUE
      IF(TIME.LE.FINTIM/2.) PRISE=0.0
      P1B=PAV
      P2B=PB2
*
*     START CALC OF INPUT AND OUTPUT PRESSURES
*
      PC1=(1.-CLOSE1)*(PRISE+P1BIAS)+CLOSE1*P1B
      PC2=(1.-CLOSE2)*(P2*Z2+P2BIAS)+CLOSE2*P2B
      PD1=.75*QS2*(TS+T-(TS**3+T**3)/3.)/AREAR
      PD2=.75*QS2*(2./3.-TS+TS**3/3.)/AREAR
      POUT1=PD1+PB2
      POUT2=PD2+PB2
      PDOUT1=(QO1/AREAR)**2
      PDOUT2=(QO2/AREAR)**2
```

```
*
*        END CALC OF INPUT AND OUTPUT PRESSURES
*
*       START CALC OF INTEGRALS FOR VOLUME AND ALL FLOWS
*
        QS =INTGRL(QSO ,CONV*(1.0-PSY-QS*ABS(QS)/CS**2)/(LS*B02)*CS)
        QC1=INTGRL(QC10,CONV*(PC1-P1B-RC1*QC1*ABS(QC1))/(LC*B02)*D1)
        QC2=INTGRL(QC20,CONV*(PC2-P2B-RC2*QC2*ABS(QC2))/(LC*B02)*D2)
        LV=2.*LGTHV*SQRT(RV1)
        QV1=FCNSW(E,0.,0.,QV1I)
        ARGQV1=CONV*(PV1-PB1-RV1*QV1*ABS(QV1))/(LV*B02)
        QV1DOT=FCNSW(E,0.,0.,ARGQV1)
        QV1I=INTGRL(QV10,QV1DOT)
        V=INTGRL(VO,CONV*(QC1-QE1+QR1+QV1)/B02)
        QV2=INTGRL(QV20,CONV*(PV2-PB2-RV2*QV2*ABS(QV2))/(LV*B02))
        QO1=INTGRL(QO10,CONV*(PD1+PB2-PO1-RO1*QO1*ABS(QO1))/(LO*B02))
        QO2=INTGRL(QO20,CONV*(PO2-PD2-PB2-RO2*QO2*ABS(QO2))/(LO*B02))
*
*        END CALC OF INTEGRALS FOR VOLUME AND ALL FLOWS
*
*       SWITCH CRITERION
*
        LSP=2.*SB
        IF(LSP.LT.SPL) GO TO 2000
        RT=1.0
  2000  CONTINUE
SORT
TITLE RESPONSE OF A TURBULENT REATTACHED JET IN AN AMPLIFIER WITH OUTPUT
INTEG MILNE
RELERR V=.001
CONTRLFINTIM=.04
FINISH RT=1.
CONST PI=3.1416,   C1=.4543,      C2=.2752
RANGE CLOSE1,CLOSE2,QC1,QC2,PB1,PB2,PAV,PC1,RE,TAUTR,AREAR,QS,QO2,WL,...
      PLEVEL,XCL,THETA,UPLUS,QV1A,QV1,QV2,V,SIGMA,DPDT
PRINT  1.E-4,TNOND,XAP,LSP,QC1,QC2,QO1,QO2,PDOUT1,PDOUT2
INCON THETAO=0.60000,  VO=6.0000,  QSO=1.0000,  QC10=0.0000,          ...
      QC20=0.0000,      QV10=0.0000,QV20=0.2000, QO10=2.0000,         ...
      QO20=0.5000,      PLEVELO=0.2000
*
*  MODEL 1
*
PARAM L=0.,          SIGMA=10.0,     RHO=1.2059,     NU=1.4864E-5,    ...  1
      PRE1=1.0,      PRE2=1.0,       POST1=0.0,      POST2=1.0,       ...  2
      D=0.905,                                                        ...
      PO=10.0,CS=0.85 ,                                               ...  4
      P1=.00,                                                         ...  5
      P2=.00,                                                         ...  6
      BO=2.1E-3,    BC=1.0,         ALPH=.20944,    XV1= 8.640,       ...
      P1BIAS=0.0,P2BIAS=0.0,PV1=0.0,PV2=0.0,PO1=0.0,PO2=0.0 ,         ...
      LGTHC=10.0,AREAC=2.0,LGTHS=15.0,AREAS=3.0,LGTHV=10.,AREAV=1.95,...
      SPL=10.0 ,LGTHR=27.75
PARAM TRISE=1.5E-3
PARAM CDMAX=.9000,CDMIN=.6000
END
*
*  FOR MODEL 1 INPUT CONTROL AMPLITUDES VA>IED FROM 0. TO 0.5 FOR BOTH
*  INACTIVE CONTROL OPEN AND BLOCKED
*
*  MODEL 2
```

```
*
TITLE RESPONSE OF A  LAMINAR  REATTACHED JET IN AN AMPLIFIER WITH OUTPUT
PRINT  5.E-3,TNOND,XAP,LSP,QC1,QC2,QO1,QO2,PDOUT1,PDOUT2
CONTRLFINTIM=4.0E-1
PARAM L=1.,           RHO=1.2059,     NU=1.4864E-5,                        ... 1
      PRE1=1.0,       PRE2=1.0,       POST1=0.0,      POST2=1.0,           ... 2
      D=0.5,                                                               ... 3
      PO=3.3333E-2,CS=.8,                                                  ...
      BO=2.0E-3,  BC=1.0,             ALPH=.20944,    XV1= 9.000,          ...
      LGTHC=10.0,AREAC=2.0,LGTHS=15.0,AREAS=3.0,LGTHV=10.0,AREAV=2.0,...  9
      SPL=10.                                                               10
END
*
*  THE LAMINAR MODEL WAS RUN FOR BOTH INACTIVE CONTROL OPEN AND BLOCKED
*  FOR RAMP PRESSURE SIGNALS TO P1=.5 WITH RISE TIMES FROM 30MS TO 400MS
*
TITLE RESPONSE OF A TURBULENT REATTACHED JET IN AN AMPLIFIER WITH OUTPUT
PRINT  1.E-4,TNOND,XAP,LSP,QC1,QC2,QO1,QO2,PDOUT1,PDOUT2
CONTRLFINTIM=4.0E-2
PARAM L=0.,           SIGMA=10.0,     RHO=1.2059,     NU=1.4864E-5,        ... 1
      PO=7.50,CS=0.85
END
*
*  THE TURBULENT MODEL WAS RUN FOR BOTH OPEN AND BLOCKED INACTIVE
*  CONTROLS FOR P1=0.0 TO 0.5
*
*  MODEL 3
*
PARAM TRISE=1.E-3
PARAM LGTHC=2.00
PARAM P1=.25
END
*
*  MODEL 3 WAS RUN FOR P1=.25
*
STOP

$REMOVE        SYSCK1
```

APPENDIX B

```
* AUTOSKEM IS A PROGRAM TO DRAW ELECTRONIC SCHEMATICS HOWEVER IT IS ALSO
*  USEFUL FOR DRAWINGS
*
* THE FOLLOWING LISTING IS A MODIFICATION OF THE ORIGINAL IN ORDER TO
*  SHOW THE ACTUAL TEST SIZE OF THE MODEL
*
* ATTACHED JET TEST MODEL 2 REV D   JMG  30 DEC 71
* DIMENSIONS ARE IN CENTIMETERS
* COMPUTER RECOGNIZES NUMBERS AS INCHES SO A SCALE FACTOR IS NEEDED TO
*  ADJUST DRAWING SIZE AND CONVERT DIMENSIONS
* FINAL DRAWING IS ACTUAL SIZE, SO SCALE FACTOR IS 1/2.54
*
FACTOR       0.3937
ORIGIN       0.          0.
LINE           .0000       .0000      .0000      .1000
LINE           .0000       .0000      .1000      .0000
ORIGIN       13.5        9.5
LINE        -5.0000        .0000   -5.2500       .0000
LINE        -5.0000      -.2500    -5.0000       .2500
LINE        -5.0000        .0000    7.7500       .0000
LINE         7.5000      -.2500     7.5000       .2500
LINE          .0000        .0000      .0000      .0000
LINE          .0000        .1000    -.1000       .1000
ARC          -.1000        .3500      .2500       210.000    270.000
ARC          -.9660      -.1500       .7500        30.000     90.000
LINE         -.9660        .6000   -4.0000       .6000
CIRCLE      -4.0000        .00000     .6000
LINE        -4.0000      -.6000     -.9660      -.6000
ARC          -.9660        .1500      .7500       270.000    330.000
ARC          -.1000      -.3500       .2500        90.000    150.000
LINE         -.1000      -.1000       .0000      -.1000
LINE          .0000      -.1000       .0000      -.3425
ARC          -.1000      -.3425       .1000       300.000    360.000
ARC           .0000      -.5157       .1000       120.000    180.000
LINE         -.1000      -.5157      -.1000    -2.5157
CIRCLE        .1000     -2.5157       .2000
LINE          .3000     -2.5157       .3000      -.5157
ARC           .2000      -.5157       .1000          .000     60.000
ARC           .3000      -.3425       .1000       180.000    240.000
LINE          .2000      -.3425       .2000      -.2425
LINE          .2000      -.2425     1.7607       -.5742
LINE         1.7607      -.5742     1.7607     -2.6157
LINE         1.7607     -2.6157       .0000    -7.6200
LINE          .0000     -7.6200     4.0000     -7.6200
LINE         4.0000     -7.6200     2.1607     -2.6157
LINE         2.1607     -2.6157     2.1607      -.6593
LINE         2.1607      -.6593     7.6200     -1.8197
LINE         7.6200      1.8197     2.1607       .6593
LINE         2.1607        .6593    2.1607      2.6157
LINE         2.1607      2.6157     4.0000      7.6200
LINE         4.0000      7.6200       .0000     7.6200
LINE          .0000      7.6200     1.7607      2.6157
LINE         1.7607      2.6157     1.7607       .5742
LINE         1.7607       .5742       .2000      .2425
LINE          .2000       .2425       .2000      .3425
ARC           .3000       .3425       .1000       120.000    180.000
ARC           .2000       .5157       .1000       300.000    360.000
LINE          .3000       .5157       .3000     2.5157
CIRCLE        .1000      2.5157       .2000
```

```
LINE          -.1000      2.5157     -.1000      .5157
ARC            .0000       .5157      .1000       180.000   240.000
ARC           -.1000       .3425      .1000          .000    60.000
LINE           .0000       .3425      .0000      .1000
CIRCLE       -5.0800     -6.9850      .2381
CIRCLE        6.3500     -6.9850      .2381
CIRCLE        6.3500      6.9850      .2381
CIRCLE       -5.0800      6.9850      .2381
LINE         -7.62         .0       -7.62      -7.62
LINE         -7.62       -7.62       7.62      -7.62
LINE          7.62       -7.62       7.62       7.62
LINE          7.62        7.62      -7.62       7.62
LINE         -7.62        7.62      -7.62       0.
WRITE        -6.     -3.    .214     0.   //ATT. JET   MODEL 2 REV D  //
WRITE        -6.     -3.3   .214     0.   //SCALE=1/1                 //
WRITE        -6.     -3.6   .214     0.   //JMG      30 DEC 71        //
ORIGIN      -13.5        -9.5
*
* REV A-CARD ORDER, B-ORIG ORDER, ADD CL, C-ADD DWG SCALE
* REV D-LISTING FOR APPENDIX B
END
```

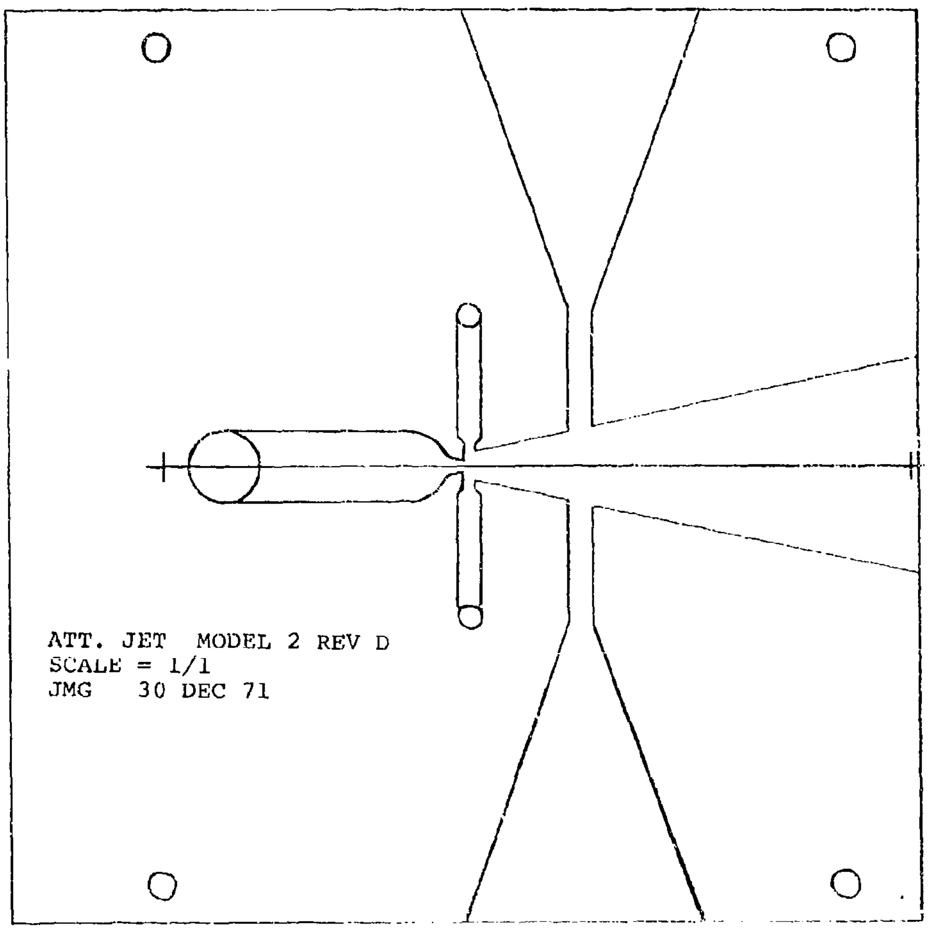

Figure B-1. Computer drawing of HDL test model.